haematologica
Journal of the Ferrata Storti Foundation

Lysine succinylation precisely controls normal erythropoiesis

by Bin Hu, Han Gong, Ling Nie, Ji Zhang, Yanan Li, Dandan Liu, Huifang Zhang, Haihang Zhang, Lu Han, Chaoying Yang, Maohua Li, Wenwen Xu, Yukio Nakamura, Lihong Shi, Mao Ye, Christopher D. Hillyer, Narla Mohandas, Long Liang, Yue Sheng and Jing Liu

Received: April 24, 2024.
Accepted: October 4, 2024.

Citation: Bin Hu, Han Gong, Ling Nie, Ji Zhang, Yanan Li, Dandan Liu, Huifang Zhang, Haihang Zhang, Lu Han, Chaoying Yang, Maohua Li, Wenwen Xu, Yukio Nakamura, Lihong Shi, Mao Ye, Christopher D. Hillyer, Narla Mohandas, Long Liang, Yue Sheng and Jing Liu. Lysine succinylation precisely controls normal erythropoiesis. Haematologica. 2024 Oct 17. doi: 10.3324/haematol.2024.285752 [Epub ahead of print]

Lysine succinylation precisely controls normal erythropoiesis

Bin Hu[#,1], Han Gong[#,1], Ling Nie[2], Ji Zhang[3], Yanan Li[1], Dandan Liu[1], Huifang Zhang[1], Haihang Zhang[1], Lu Han[1], Chaoying Yang[1], Maohua Li[1], Wenwen Xu[1], Yukio Nakamura[4], Lihong Shi[5], Mao Ye[6], Christopher D. Hillyer[7], Narla Mohandas[7], Long Liang[1,*], Yue Sheng[1,*], Jing Liu[1,*]

# These authors contributed equally to this work.

*Corresponding author: jingliucsu@hotmail.com, shengyue1900@163.com, liang_long614@126.com

[1]Department of Hematology, The Second Xiangya Hospital, Molecular Biology Research Center, School of Life Sciences, Hunan Province Key Laboratory of Basic and Applied Hematology, Central South University, Hunan, China. [2]Department of Hematology, Xiangya Hospital, Central South University, Hunan, China. [3]The Affiliated Nanhua Hospital, Department of Clinical Laboratory, Hengyang Medical School, University of South China, Hunan, China.[4]Cell Engineering Division, RIKEN BioResource Center, Tsukuba, Ibaraki, Japan. [5]State Key Laboratory of Experimental Hematology, National Clinical Research Center for Blood Diseases, Institute of Hematology & Blood Diseases Hospital, Chinese Academy of Medical Sciences & Peking Union Medical College; CAMS Center for Stem Cell Medicine, PUMC Department of Stem Cell and Regenerative Medicine, Tianjin, China. [6]Molecular Science and Biomedicine Laboratory (MBL), State Key Laboratory of Chemo/Biosensing and Chemometrics, College of Biology, College of Chemistry and Chemical Engineering, Aptamer Engineering Center of Hunan Province, Hunan University, Hunan, China. [7]Research Laboratory of Red Cell Physiology, New York Blood Center, New York, NY.

Authors' contributions

J.L., Y.S., L.L. and M.Y. conceived and designed the experiments. B.H., H.G., J.Z., Y.L., D.L., Y. C., L.H., H. Z., M. L., and W. X. performed experiments and analyzed data. L. N. collected the blood sample. Y. N. and L.S. provided the cell line. Y.S. and J.L. drafted the manuscript.

M.Y., C.H., N.M., L. L., Y.S., and J.L. provided insights into some aspects of the work and edited the manuscript. All authors read and approved the final manuscript.

Funding

This work was supported by the grants from the National Natural Science Foundation of China (Grants 81920108004, 81770107, 92253201, 81870105, 82100137, 32270791, 32350026, and 22334005), the National Key Research and Development Program of China (Grant 2021YFA0909403, 2021YFA0909400), Huxiang Youth Talent Support Program (2022RC1205), International Centre for Genetic Engineering and Biotechnology-ICGEB (CRP/CHN22-03_EC), the Natural Science Foundation of Hunan Province (2022JJ30183), Changsha Municipal Natural Science Foundation (No.kq2208382), and the Fundamental Research Funds for the Central Universities of Central South University (2021zzts0085). Pcl-20 plasmid is kindly provided by Huilin Huang.

Availability of data and material

The identified succinylated protein data have been deposited in the National Genomics Data Center (https://ngdc.cncb.ac.cn/) with the dataset identifier OMIX004702. Further inquiries may be directed to the corresponding author.

Conflicts of Interest

The authors declare that they have no competing interests.

Abstract

Lysine succinylation (Ksu) has recently emerged as a protein modification that regulates diverse functions in various biological processes. However, the systemically and precise role of lysine succinylation in erythropoiesis remains to be fully elucidated. In this study, we noted a prominent increase of succinyl-CoA and lysine succinylation during human erythroid differentiation. To explore the functional significance of succinylation, we inhibited succinylation by either knock downing key succinyltransferases or overexpressing desuccinylases. Succinylation inhibition led to suppressed cell proliferation, increased apoptosis, and disrupted erythroid differentiation. In vivo overexpression of the desuccinylases SIRT5 delayed erythroid differentiation. Furthermore, integrative proteome and succinylome analysis identifies 939 succinylated proteins with 3,562 Ksu sites, distributed across various cellular compartments and involved in multiple cellular processes. Significantly, inconsistencies between protein expression levels and succinylation levels were observed, indicating that the succinylation of certain proteins may function independently of expression. Mechanistically, we implicated KAT2A-mediated succinylation of histone H3 K79, leading to chromatin remodeling and subsequently erythropoiesis regulation. Specially, we identified CYCS as a key regulator of erythropoiesis, which depends on its succinylation sites K28/K40. Taken together, our comprehensive investigation of the succinylation landscape during erythropoiesis provides valuable insights into its regulatory role and offer potential implications for erythroid-related diseases.

Keywords: erythropoiesis, lysine succinylation, succinylome, histone H3, CYCS

Introduction

Red blood cells (RBCs), the most abundant of circulating blood cells, play crucial roles in gas exchange and in immunity (1). In a healthy adult, more than two million RBCs are generated per second through a highly regulated and complex process known as erythropoiesis (2). This process involves various cellular events, including lineage selection, morphological and structural changes, cell metabolic changes, and cell cycle regulation (3-5). Following commitment to erythroid lineage, hematopoietic stem cells (HSCs) generate the early erythroid progenitor, burst-forming unit-erythroid (BFU-E) cells. These BFU-E cells further develop into colony-forming unit-erythroid (CFU-E) cells that undergo terminal erythroid differentiation. During terminal erythroid differentiation, proerythroblasts, undergo 4 or 5 mitotic divisions to generate sequentially differentiate into basophilic, polychromatic, and orthochromatic erythroblasts. Finally, the orthochromatic erythroblasts enucleate to generate reticulocytes (6, 7). Disordered erythropoiesis is a critical feature of human diseases such as thalassemia's, congenital dyserythropoietic anemias, and myelodysplastic syndromes (8).

Previous studies have established essential roles of transcription factors and cytokine-mediated signal transduction in regulating erythropoiesis, including GATA1 (9), KLF1 (10), and TAL1 (11) as well as EPO (12) and TGF-β (13). With the emergence of the post-genome era, post-translational modifications (PTMs) of proteins, which includes methylation, acetylation, phosphorylation, and ubiquitination, have increasingly become an area of active investigation within the field of erythroid development (7, 14-19). For example, HDAC5 was reported to regulate chromatin remodeling in late-stage erythroblasts by affecting H4 acetylation (7). GATA1 can be stabilized by the deubiquitylase USP7 to regulate human terminal erythroid differentiation (19). Phosphorylated proteins have been mapped the regulatory network during human erythroid differentiation (15, 16). These studies increase our understanding of post□transcriptional and translational mechanisms during erythroid development. However, the precise and systematical roles of additional PTMs in erythropoiesis remains to be largely defined.

With recent technological advances, novel methods for analyzing protein post-translational

modifications have been developed. Lysine succinylation, a recently recognized reversible modification, has garnered a lot of attention. This modification involves the covalent addition of succinyl groups to lysine residues, resulting in change of protein charge from positive to negative, along with associated structural alterations (20). The level of succinylation is precisely regulated by succinylation donors, lysine desuccinylases, and succinyltransferases (21). Disruptions in succinylation has been linked to diverse diseases, including abnormal stem cell development (22), tumors (23), cardiac metabolic diseases (24), and nervous system disorders (25). However, the role of lysine succinylation in erythropoiesis has not been elucidated.

In the present study, we evaluated changes in succinylation levels during erythroid differentiation in vitro and in vivo and showed that decreased in succinylation levels disrupt cell proliferation and differentiation, as well as induce apoptosis. Using mass spectrometry, we identified a comprehensive list of succinylated proteins at both early and late stages of erythroid differentiation and uncovered the molecular mechanisms of regulation of erythropoiesis by succinylation. These findings contribute to our increased understanding of novel post-translational modifications involved in regulation of erythropoiesis.

Methods

Antibodies and reagents

All antibodies and reagents used for flow cytometry, western blot (WB), and immunofluorescence analyses are listed in supplemental Table 1 and supplemental Table 2.

Ethical approval

Human blood samples were acquired from Xiangya Hospital with the approval of the Ethics committee. Informed consent was obtained from all participating subjects as well as their guardians, when applicable. Animal experiments were performed according to protocols approved by the Animal Ethics Committee of Xiangya Hospital.

In vitro differentiation of $CD34^+$ cells and HUDEP2 cells towards erythroid lineage

Our previous research had described the culture medium composition and differentiation protocol of $CD34^+$ cells from peripheral blood mononuclear cells induced to undergo erythroid differentiation (5). Human Umbilical Cord Derived Erythroid Progenitor Cell (HUDEP2) cell line originated from Tianjin Blood Research Institute and induced to undergo erythroid differentiation as per previously described protocol (26).

Cytospin preparation

A total of 1×10^5 cells in 100 μL DPBS were spun for 5 minutes at 400 rpm onto glass slides using the cytospin apparatus. After airdrying for 1 minute, slides were stained with Giemsa staining solution (Sigma, Darmstadt, Germany) according to manufacturer's instructions. Stained cells were viewed, and images were acquired with an Olympus BX51 microscope and QCapture Pro 6.0 (Tokyo, Japan).

Plasmid construction, virus preparation and cell infection

Plasmid construction, viral packaging of target genes, and cell infection procedures were conducted using established protocols described in our previous studies (27). The sequences of shRNAs used are listed in supplemental Table 3.

Bone marrow (BM) transplantation

BM transplantation was performed using 6–8-week-oldC57BL6 mice. The mice were intraperitoneally injected with 150 mg/kg of 5-fluorouracil (5-Fu) to ablate endogenous hematopoietic stem cells. After 5 days, the mice were sacrificed and BM cells were harvested. The BM cells were infected with either the MigR1 retrovirus (containing IRES-GFP) or the MIGR-SIRT5 retrovirus. The infected BM cells were then transplanted into sublethally irradiated 6–8-week-oldrecipient C57BL6 mice via retro-orbital injection. For lineage tracing experiments, doxycycline (2 mg/ml) and sucrose (10 mg/ml) were added to the drinking water of recipient mice prior to transplantation and maintained throughout the study.

LC-MS/MS-based analysis of coenzyme A

Cells at different stages of differentiation were obtained as previously described (28). Mass

spectrometry was used to detect levels of coenzyme A in the cells.

Bioinformatics analysis

The succinylated peptides or proteins with valid intensities in at least two replicates were selected for subsequent analysis. We set the criteria for differential proteins/sites as |log2 fold change|>0.5 and p-value<0.05 (25, 29). Functional annotation of the identified proteins was carried out using the online platform Proteomaps (https://www.proteomaps.net/) (30). The Motif-X algorithm was applied to analyze motif characteristics within the 10 amino acid residues preceding and following lysine residues (31). Enrichment analysis was performed using the clusterProfiler package (32) and the DAVID tool (33). Subcellular localization data for proteins were retrieved from The Human Protein Atlas (https://www.proteinatlas.org/). To visualize pathway enrichment outcomes, Cytoscape (v3.9.0) and the EnrichmentMap (34) application were used.

Statistical analysis

Statistical analysis is derived from three independent experiments, and the bar plot represents the mean ± SD of triplicate samples. Unless otherwise specified, differences between different subgroups were assessed using Student's t test. Statistical tests, calculations, and visualizations were primarily conducted using R software (v4.0.3) or GraphPad Prism 8 software.

Results

Succinylation is increased during erythropoiesis

Acyl-CoAs, essential metabolic intermediates derived primarily from glucose, fatty acids, and amino acids, exert a significant influence on post-translational modifications by adding acyl groups to lysine residues of proteins and modulate their functions (35). To investigate the potential role of acyl-CoAs in erythropoiesis, we initially conducted targeted metabolomics to assess the concentrations of different acyl-CoA types in Day 4 (early stage) and Day 13 (late stage) erythroid cells (Figure 1A). Our investigation revealed the presence of various common acyl-CoAs, including acetyl-, succinyl-, malonyl-, crotonyl-, butyryl-, and propionyl-CoA, in

human erythroid cells. Interestingly, we noticed that succinyl-CoA levels were most abundant and significantly upregulated during erythroid differentiation (Figure 1B). Subsequently, our inquiry extended to examining whether protein succinylation levels mirrored the observed succinyl-CoA dynamics. WB showed a progressive rise in succinylation levels during erythroid differentiation of human $CD34^+$ cells (Figure 1C), whereas other post-translational modifications, such as methylation and acetylation, remained largely unchanged (Supplemental Figure S1A-F). Furthermore, we corroborated this observation using HUDEP2 cells, an erythroid progenitor cell line derived from $CD34^+$ cells (Figure 1D). To comprehensively assess the subcellular distribution of succinylation throughout erythroid differentiation, we performed immunofluorescence imaging on nuclear and cytoplasmic fractions. A robust increase of succinylation was seen in both compartments (Figure 1E-H). Collectively, these dynamic changes in the levels of succinylation suggest the important role in erythropoiesis.

Disruption of lysine succinylation impairs human erythroid differentiation

Recent findings have documented that succinyltransferases and desuccinylases, including CPT1A (36), HAT1 (37), KAT2A (38), SIRT5 (39) and SIRT7 (40), are key regulators of succinylation. To investigate the importance of succinylation within erythroid differentiation, we employed an shRNA-mediated knockdown approach or a lentiviral method for overexpression to interfere with this process. The qPCR results showed that the mRNA levels of these succinyltransferases and desuccinylases were significantly decreased (Figure S2A). Knockdown of succinyltransferases CPT1A, HAT1, and KAT2A resulted in decreased succinylation levels in HUDEP2 cells (Figure 2A). This reduction was accompanied by inhibition of cell proliferation, cell cycle arrest, induction of apoptosis and blockage of erythroid differentiation (Figure 2B-E). Similarly, reduction of succinylation by overexpression of desuccinylases SIRT5 and SIRT7 led to comparable consequences. Furthermore, we disrupted succinylation in human $CD34^+$ cells by knocking down KAT2A or overexpressing SIRT5, resulting in impaired erythroid development (Supplemental Figure S2B-H). Consistent with these findings, treatment with three succinyltransferase inhibitors (Butyrolactone-3, Etomoxir, and JG-2016) produced similar results (Supplemental Figure

S3A-E).

Overexpression of the desuccinylases SIRT5 delays erythroid differentiation in vivo

Our bulk RNAseq data suggested that among enzymes related to protein succinylation modification, SIRT5 expression is relatively low during erythroid differentiation (Supplemental Figure S4A) (41). Analysis of public scRNA-seq data from BM samples (42) corroborated this finding, showing low SIRT5 expression in the erythroid lineage (Supplemental Figure S4B). Additionally, SIRT5 is extensively employed as a tool for investigating protein succinylation in vivo (24, 43, 44). Therefore, we conducted a BM transplantation study in lethally irradiated B6 recipient mice, wherein retroviral transduction of the expression vector (MigR1) or OV-SIRT5 was utilized. The overall experimental process was shown in Supplemental Figure S4C. Four weeks post-transplantation, we assessed the SIRT5 expression and succinylation levels in mouse BM cells, revealing a significant reduction in succinylation levels in the BM cells of OV-SIRT5 mice compared to Vectors (Figure 3A, Supplemental Figure S4D). Blood cell count analysis further demonstrated that red blood cell (RBC) count and hemoglobin levels were significantly lower in OV-SIRT5 mice compared to Vectors, while white blood cells (WBC) were no significant differences (Figure 3B). Skeletal examination of the lower limbs revealed a noticeable pallor in the bones of OV-SIRT5 mice when compared to the control mice (Figure 3C). This distinction was also observed in the BM cell pellets. Moreover, the BM cell count indicated a significantly lower number of cells in OV-SIRT5 mice compared to the control group (Supplemental Figure S4E). Flow cytometric analysis confirmed that overexpression of SIRT5 reduced the proportion of Ter-119^{+} erythroid cell among BM GFP^{+} cells (Figure 3D, Supplemental Figure S4F). Furthermore, we performed immunohistochemical staining on the BM, and we found that after SIRT5 overexpression, the expression of TER119 in the BM was reduced, and there was no significant difference in the expression of other lineage-specific makers (Figure 3E, Supplemental Figure S4G). Subsequently, we distributed erythroblasts into five sub-populations based on the surface marker levels of CD44 (45). Notably, Flow cytometry analysis showed that SIRT5 overexpression induced mildly ineffective erythropoiesis, as reflected by decreased–reticulocytes in BM (Figure 3F). Together the

findings in vivo and in vitro, our results imply that the accurate expression of succinylation plays a crucial role in erythroid development.

The succinylome and proteome of differentiating erythroid cells

To obtain insights into proteins succinylation and their participation in regulating erythroid differentiation, we embarked on proteome and succinylome analyses of differentiating HUDEP2 cells (Figure 4A). PCA analysis showed the reproducibility of the two omics datasets (Supplemental Figure S5A). In total, we identified 58,454 peptides corresponding to 6,132 proteins as well as 3,540 succinylated peptides from 939 unique proteins (Figure 4B). We further noted that nearly all succinylated proteins were also present in the proteomes of the same samples. Evidently, the majority (95.7%) of the commonly succinylated proteins were shared between the early-stage and late-stage of erythroid differentiation in the succinylome, indicating that erythroid differentiation requires alteration of succinylation instead of de novo modification (Figure 4B). The degree of protein succinylation was significantly increased at late-stage of erythroid differentiation (Figure 4C), which was consistent with the observed phenotype in Figure 1C and 1D. Contrast, the expression of protein levels was decreased in erythroid differentiation (Supplemental Figure S5B). The most abundant succinylated proteins included hemoglobin and mitochondria-related proteins (Figure 4C). Notably, Spearman's analysis revealed inconsistencies between alterations in protein levels and succinylation levels ($R = -0.103$) (Figure 4D). Proteomaps analysis of the total proteins revealed a significantly higher proportion of hemoglobin proteins and lower levels of cell cycle proteins in the late-stage of erythroid differentiation (Supplemental Figure S5C).

To investigate the sequence patterns of succinylation during erythroid differentiation, we identified eight conserved motifs from all succinylated peptides (Supplemental Figure S6A). We quantified the occurrence of succinylation sites and observed that approximately 60% of the proteins contained two or more succinylation sites (Figure 4E). Furthermore, we performed GO enrichment analysis on proteins with more than 10 succinylation sites and identified significant enrichment in pathways such as respiratory electron transport, ATP

synthesis, and other related processes (Supplemental Figure S6B). To assess the specificity of proteins with over 10 succinylation sites, we compared our findings with succinylation data from Alzheimer's disease (AD) patients (25) as a non-erythroid reference (Supplemental Figure S6C). Interestingly, while there was some overlap, we found that highly succinylated proteins in our cohort were enriched in the erythroid lineage. In contrast, proteins highly succinylated in AD patients were predominantly associated with mitochondrial metabolism, such as ALDH7A1. We ectopically expressed HBB and ALDH7A1 in $CD34^+$ cells, observing that HBB was significantly more succinylated in late erythroid cells than in early cells (Supplemental Figure S6D). IP results showed that HBB interacted with CPT1A but not with HAT1 or KAT2A (Supplemental Figure S6D). Although ALDH7A1 exhibited detectable succinylation when overexpressed, it did not significantly interact with CPT1A, KAT2A, or HAT1 (Supplemental Figure S6E). This specificity may reflect the distinct metabolic and functional requirements of different cellular processes, such as erythroid development versus neurodegenerative diseases.

Additionally, we noted that proteins with multiple Ksu sites (N > 2) exhibited more succinylation modification at the late-stage of erythroid differentiation (Supplemental Figure S6F), such as SLC4A1, SPTA1, and SPTB. The WB experiments indicated that these proteins had high succinylation levels (Supplemental Figure S6G). We further investigated the distribution and role of succinylated proteins by conducting a cellular compartment analysis of the 939 quantifiable succinylated proteins. Our findings revealed that succinylated proteins are present in various subcellular compartments (Figure 4F). Markedly, approximately 33.8% (317/939) of the succinylated proteins were localized in the mitochondria, including CYCS, SDHA, and LDHA. In the cytoplasm, the succinylated proteins displayed significant enrichment in processes such as translational initiation, mRNA catabolic processes, and protein targeting to the endoplasmic reticulum (Supplemental Figure S6H). The succinylated proteins localized in the nucleus showed significant enrichment in the regulation of mRNA metabolic processes, DNA conformation changes, and hematopoietic stem cell differentiation (Supplemental Figure S6H). Additionally, the succinylated proteins in the mitochondria were significantly enriched in mitochondrial gene expression, translation, and ATP metabolic

processes (Supplemental Figure S6H). The succinylated proteins in the others (membrane, vesicles, endoplasmic reticulum, etc.) were significantly enriched in endosomal transport, response to endoplasmic reticulum stress, and positive regulation of cell adhesion (Supplemental Figure S6H). These results collectively suggest a potential regulatory role of succinylation during erythroid differentiation.

Comparison of the succinylome during early-stage and late-stage of erythroid differentiation

We then investigated the dynamic alterations in succinylation during erythroid differentiation. The volcano plot indicated 339 upregulated Ksu sites along with 318 downregulated Ksu sites (Figure 5A), distributed across the nucleus, cytosol, and mitochondria (Figure 5B). Importantly, GO analysis of the upregulated succinylated proteins demonstrated enrichment in processes critical for erythroid development, including regulation of hemopoiesis, erythrocyte differentiation, and erythrocyte homeostasis (Figure 5C). This enrichment underscores the potential importance of protein succinylation in regulating red blood cell development and function. Conversely, downregulated succinylated proteins exhibited enrichment in metabolic processes such as ribonucleotide biosynthetic processes, small molecule catabolic processes, and fatty acid metabolic processes (Figure 5D), suggesting a shift in cellular metabolism during differentiation. To further reveal the pivotal pathways involving succinylated proteins, we constructed a functional enrichment network (Figure 5E). This analysis reinforced our findings, revealing enrichment in pathways related to hematopoiesis and heme synthesis, including erythrocyte differentiation and homeostasis. Collectively, these results highlight the impact of succinylome changes on erythroid differentiation and its associated pathways, pointing to a potential regulatory mechanism in erythropoiesis mediated by protein succinylation.

Association analysis of succinylome and proteome

Given the prevalence of succinylated proteins within mitochondria, we undertook an investigation into the relationship between alterations in metabolism-related protein levels and succinylation levels. As depicted in Figure 6A, a substantial subset of succinylated proteins

participated in the pivotal metabolic pathways of erythropoiesis, that included glycolysis, oxidative phosphorylation, the TCA cycle, and heme synthesis. Furthermore, we performed a global association analysis of the fold change in succinylation levels and protein levels (Figure 6B). Remarkably, the overall correlation between the fold changes of the two omics was very weak (R = -0.06). We selected the top 10 succinylated proteins (including histone H3, CYCS, XPNPEP1, GUF1, FDPS, TARS2, NT5C, ECI2, ATP5F1D, and POLDIP2) to visualize using a heatmap, and the results supported the notion that changes in succinylation of these proteins were independent of variations in protein abundance (Figure 6C).

The genome loci of H3K79Ksu mediated by KAT2A in CD34$^+$ cells.

As the histone H3, which was succinylated by succinyltransferase KAT2A (38), was the most succinylated proteins depicted in the above proteins, we investigated the role of succinylation in H3K79 during erythroid differentiation. WB confirmed the succinylation levels of H3K79 (H3K79Ksu) were significantly increased during erythroid differentiation (Figure 7C, Supplemental Figure S7A, B). Co-immunoprecipitation (Co-IP) proved the interaction between KAT2A and histone H3 in HUDEP2 cells (Figure 7B). Additionally, WB results demonstrated that KAT2A knockdown reduced the H3K79Ksu (Figure 7C, Supplemental Figure S7C-E).

To further elucidate the role of H3K79Ksu in the erythrocytes, we performed CUT&Tag of H3K79Ksu after KAT2A knockdown. The normalized density showed that KAT2A knockdown significantly reduced the genomic binding capacity of H3K79Ksu (Figure 6F). Genomic annotation of the affected peaks showed their distribution as follows: 13% in promoters, 31.4% in other intron, and 37.6% in distal intergenic (Supplemental Figure S7F). Representative erythroid gene loci demonstrating H3K79Ksu signal changes after KAT2A knockdown were shown in Figure 6G. Intersection analysis of peaks located in promoter regions identified a total of 2,511 peaks (Supplemental Figure S7G). Enrichment analysis revealed that these peaks were associated with transcription factor binding, nuclear envelope, and chromatin remodeling processes (Figure 7F). Previous studies suggested that histones participate in chromatin condensation, enucleation, and reticulocyte maturation processes (46).

To further investigate this, we conducted a ChIP-qPCR experiments using a H3K79 Ksu Ab. Our results suggested that the reduced H3K79Ksu was specifically enriched in genes associated with chromatin remodeling, including XPO7, FOXO3, HDAC6, CLTA, and HNRNPU after KAT2A knockdown (Figure 6H). These findings imply that proteins succinylation mediated by succinyltransferase plays an important role in erythroid differentiation.

Succinylation is required for CYCS functions in erythropoiesis

Previous literature (47) and our results suggest that proteins with multiple succinylation sites are abundant in mitochondria. Accordingly, we chose cytochrome C (CYCS), which exhibited the most pronounced change in succinylation in mitochondria, for further analysis. CYCS plays a crucial role as an electron carrier in biological oxidation and cellular respiration (48). Abnormal function of CYCS leads to blood cell-related disease (49). To investigate the function and succinylation of CYCS during erythroid differentiation, we conducted shCYCS and succinylation-deficient mutations of CYCS (K28R and K40R) in the modified residues. The WB confirmed the efficacy of shCYCS and the WT-flag-CYSC or the mutations, and IP assay showed that succinylation levels were downregulated when either K28 or K40 or both were mutated compare to WT-flag-CYCS (Figure 8A). Functionally, knockdown of CYCS led to inhibition of cell proliferation, blocked erythroid differentiation, induced cell apoptosis, and decreased mitochondrial membrane potential (Figure 8B-F, Supplementary Figure S8). Notably, the overexpression of WT-flag-CYCS rescued these phenotypes of shCYCS but not succinylation-deficient mutants. In summary, these findings reveal that CYCS function depends on succinylation in coordinating erythroid differentiation.

Discussion

Our primary findings are illustrated in Figure 8G. In this study, we discovered that succinylation gradually increases during erythroid differentiation. Disrupting succinylation levels resulted in aberrant erythroid development. Using multi-omics to analyze dynamic changes in the succinylation network, we identified 3,562 succinylation modification sites and 939 succinylated proteins. These proteins are predominantly involved in crucial pathways for

erythroid development, including mitochondrial metabolism, heme synthesis, and chromatin remodeling.

During erythroid differentiation, erythrocytes undergo remodeling such that mature erythrocytes mainly contain hemoglobin as their protein component. To achieve this, approximately 10^9 molecules of hemoglobin must be synthesized, requiring the consumption of 10^{10} molecules of succinyl-CoA (50). The interaction of succinyl-CoA with the erythroid-specific ALAS-E gene is disrupted in sideroblastic anemia (51). Furthermore, IDH1 mutations can alter downstream succinyl-CoA levels, contributing to the onset and progression of myelodysplastic syndromes (MDS) (52). In humans, heme and globin synthesis predominantly occur in basophilic erythroblasts, with synthesis levels peaking in polychromatic/orthochromatic erythroblasts (41, 50). Interestingly, our LS/MS data indicate that succinyl-CoA exhibits the highest abundance among various acyl-CoAs and maintains elevated levels throughout terminal erythroid differentiation. Notably, elevated succinyl-CoA levels can result in lysine succinylation of proteins. Succinylation has been suggested to play a role in the regulation of a wide range of biological processes (20). Although the importance of protein succinylation in pathological conditions has been recognized, such as leukemia (53), its role in normal blood development has not been extensively studied. Our study represents the first demonstration that succinyl-CoA serves additional functions during erythropoiesis beyond heme synthesis. We further reveal that succinylation mediated by succinyl-CoA gradually increases during the terminal stages of erythroid differentiation and plays a crucial role.

Protein succinylation levels are regulated by succinyltransferases and desuccinylases. Many of these enzymes have been shown to regulate both succinylation and acetylation, such as KAT2A, HAT1, and SIRT5 (54). There are also bifunctional enzymes unrelated to acetylation, such as CPT1A (55, 56). Interestingly, when we knocked down succinyltransferases or overexpressed desuccinylases in terminal erythroblasts, both manipulations showed similar phenotypes, inhibiting terminal cell proliferation and differentiation. Among these succinylation-related enzymes, SIRT5 has been reported to have relatively weak deacetylase

activity compared to other sirtuins. In fact, SIRT5 exhibits robust desuccinylation activity approximately 1,000-fold higher catalytic efficiency than its deacetylation activity (39, 57). Therefore, SIRT5 is commonly used in succinylation studies due to its preference for desuccinylation over deacetylation. Furthermore, our investigation revealed that SIRT5 expression remains consistently low across erythroid differentiation stages (Supplementary Figure S2), and the phenotype of KO-Sirt5 mice does not exhibit disruption in erythroid development (58). To deepen our understanding of succinylation, we conducted in vivo transplantation experiments in mice by overexpressing SIRT5. Remarkably, this overexpression significantly altered the succinylation patterns of intracellular proteins, resulting in impaired erythroid differentiation and decreased red blood cell production in vivo. These findings in vivo and in vitro underscore the precise regulation of succinylation during erythroid differentiation. Any disturbance in this balance could potentially contribute to erythroid developmental disorders and the onset of erythroid-related diseases (59).

Prior investigations have predominantly linked succinylation to mitochondrial metabolic enzymes (60, 61). However, subcellular localization analysis of our data reveals that numerous succinylated proteins exhibit distribution across cellular compartments, including the nucleus and plasma. Our findings indicate that succinylation in the nucleus is enriched in pathways such as chromatin remodeling and DNA synthesis, while in the cytoplasm, it predominantly enriches processes like translation initiation, translocation, and protein synthesis. This suggests the pivotal role of succinylation as a functional modification in erythroid differentiation. Furthermore, our analysis highlights the close association of these protein modifications with erythrocytes; many succinylated proteins are associated with erythrocyte functions, particularly within the hemoglobin family. Notably, succinylated forms of hemoglobin comprise 80% of common hemoglobin family members. Remarkably, the succinylation sites we identified align with pathogenic mutation sites reported in HBB and HBA in thalassemia, suggesting a potential role of succinylation in regulating hemoglobin's normal function (62, 63). We will pursue future studies investigating the relationship between succinylation modification and related diseases.

In conclusion, our results establish a bridge between succinylation and erythropoiesis. The quantitative and modification proteomic analyses of the succinylation proteins change during erythropoiesis. Succinylation was found to have an important function in erythroid differentiation, our study providing new mechanistic insights into normal and disordered erythropoiesis.

References

1. Xu C, He J, Wang H, et al. Single-cell transcriptomic analysis identifies an immune-prone population in erythroid precursors during human ontogenesis. Nat Immunol. 2022;23(7):1109-1120.
2. Caulier AL, Sankaran VG. Molecular and cellular mechanisms that regulate human erythropoiesis. Blood. 2022;139(16):2450-2459.
3. Hattangadi SM, Wong P, Zhang L, Flygare J, Lodish HF. From stem cell to red cell: regulation of erythropoiesis at multiple levels by multiple proteins, RNAs, and chromatin modifications. Blood. 2011;118(24):6258-6268.
4. Han X, Zhang J, Peng Y, et al. Unexpected role for p19INK4d in posttranscriptional regulation of GATA1 and modulation of human terminal erythropoiesis. Blood. 2017;129(2):226-237.
5. Wang Z, Wang P, Zhang J, et al. The novel GATA1-interacting protein HES6 is an essential transcriptional cofactor for human erythropoiesis. Nucleic Acids Res. 2023;51(10):4774-4790.
6. Hu J, Liu J, Xue F, et al. Isolation and functional characterization of human erythroblasts at distinct stages: implications for understanding of normal and disordered erythropoiesis in vivo. Blood. 2013;121(16):3246-3253.
7. Wang Y, Li W, Schulz VP, et al. Impairment of human terminal erythroid differentiation by histone deacetylase 5 deficiency. Blood. 2021;138(17):1615-1627.
8. Cazzola M. Ineffective erythropoiesis and its treatment. Blood. 2022;139(16):2460-2470.
9. Crispino JD. GATA1 in normal and malignant hematopoiesis. Semin Cell Dev Biol. 2005;16(1):137-147.
10. Nuez B, Michalovich D, Bygrave A, Ploemacher R, Grosveld F. Defective haematopoiesis in fetal liver resulting from inactivation of the EKLF gene. Nature. 1995;375(6529):316-318.
11. Shivdasani RA, Mayer EL, Orkin SH. Absence of blood formation in mice lacking the T-cell leukaemia oncoprotein tal-1/SCL. Nature. 1995;373(6513):432-434.
12. Kuhrt D, Wojchowski DM. Emerging EPO and EPO receptor regulators and signal transducers. Blood. 2015;125(23):3536-3541.
13. Gao X, Lee HY, da Rocha EL, et al. TGF-beta inhibitors stimulate red blood cell production by enhancing self-renewal of BFU-E erythroid progenitors. Blood. 2016;128(23):2637-2641.
14. Li M, Liu D, Xue F, et al. Stage-specific dual function: EZH2 regulates human erythropoiesis by eliciting histone and non-histone methylation. Haematologica. 2023;108(9):2487-2502.
15. Karayel O, Xu P, Bludau I, et al. Integrative proteomics reveals principles of dynamic phosphosignaling networks in human erythropoiesis. Mol Syst Biol. 2020;16(12):e9813.
16. Peng Y, Tang L, Li Y, et al. Comprehensive proteomic analysis reveals dynamic phospho-profiling in human early erythropoiesis. Br J Haematol. 2022;199(3):427-442.
17. Nguyen AT, Prado MA, Schmidt PJ, Min M, et al. UBE2O remodels the proteome during terminal erythroid differentiation. Science. 2017;357(6350):eaan0218.
18. Xu P, Scott DC, Xu B, et al. FBXO11-mediated proteolysis of BAHD1 relieves PRC2-dependent transcriptional repression in erythropoiesis. Blood. 2021;137(2):155-167.

19. Liang L, Peng Y, Zhang J, et al. Deubiquitylase USP7 regulates human terminal erythroid differentiation by stabilizing GATA1. Haematologica. 2019;104(11):2178-2187.
20. Zhang Z, Tan M, Xie Z, et al. Identification of lysine succinylation as a new post-translational modification. Nat Chem Biol. 2011;7(1):58-63.
21. Shang S, Liu J, Hua F. Protein acylation: mechanisms, biological functions and therapeutic targets. Signal Transduct Target Ther. 2022;7(1):396.
22. Huang LY, Ma JY, Song JX, et al. Ischemic accumulation of succinate induces Cdc42 succinylation and inhibits neural stem cell proliferation after cerebral ischemia/reperfusion. Neural Regen Res. 2023;18(5):1040-1045.
23. Lu K, Han D. A review of the mechanism of succinylation in cancer. Medicine (Baltimore). 2022;101(45):e31493.
24. Sadhukhan S, Liu X, Ryu D, et al. Metabolomics-assisted proteomics identifies succinylation and SIRT5 as important regulators of cardiac function. Proc Natl Acad Sci U S A. 2016;113(16):4320-4325.
25. Yang Y, Tapias V, Acosta D, et al. Altered succinylation of mitochondrial proteins, APP and tau in Alzheimer's disease. Nat Commun. 2022;13(1):159.
26. Kurita R, Suda N, Sudo K, et al. Establishment of immortalized human erythroid progenitor cell lines able to produce enucleated red blood cells. PLoS One. 2013;8(3):e59890.
27. Sheng Y, Yu C, Liu Y, et al. FOXM1 regulates leukemia stem cell quiescence and survival in MLL-rearranged AML. Nat Commun. 2020;11(1):928.
28. Neubauer S, Chu DB, Marx H, Sauer M, Hann S, Koellensperger G. LC-MS/MS-based analysis of coenzyme A and short-chain acyl-coenzyme A thioesters. Anal Bioanal Chem. 2015;407(22):6681-6688.
29. Liu Q, Wang H, Zhang H, et al. The global succinylation of SARS-CoV-2-infected host cells reveals drug targets. Proc Natl Acad Sci U S A. 2022;119(30):e2123065119.
30. Liebermeister W, Noor E, Flamholz A, Davidi D, Bernhardt J, Milo R. Visual account of protein investment in cellular functions. Proc Natl Acad Sci U S A. 2014;111(23):8488-8493.
31. Bailey TL, Johnson J, Grant CE, Noble WS. The MEME Suite. Nucleic Acids Res. 2015;43(W1):W39-49.
32. Yu G, Wang LG, Han Y, He Q-Y. clusterProfiler: an R package for comparing biological themes among gene clusters. OMICS. 2012;16(5):284-287.
33. Sherman BT, Hao M, Qiu J, et al. DAVID: a web server for functional enrichment analysis and functional annotation of gene lists (2021 update). Nucleic Acids Res. 2022;50(W1):W216-W221.
34. Merico D, Isserlin R, Stueker O, Emili A, Bader GD. Enrichment map: a network-based method for gene-set enrichment visualization and interpretation. PLoS One. 2010;5(11):e13984.
35. Trefely S, Lovell CD, Snyder NW, Wellen KE. Compartmentalised acyl-CoA metabolism and roles in chromatin regulation. Mol Metab. 2020;38:100941.
36. Kurmi K, Hitosugi S, Wiese EK, et al. Carnitine Palmitoyltransferase 1A Has a Lysine Succinyltransferase Activity. Cell Rep. 2018;22(6):1365-1373.
37. Yang G, Yuan Y, Yuan H, et al. Histone acetyltransferase 1 is a succinyltransferase for histones and non-histones and promotes tumorigenesis. EMBO Rep. 2021;22(2):e50967.
38. Wang Y, Guo YR, Liu K, et al. KAT2A coupled with the alpha-KGDH complex acts as a

histone H3 succinyltransferase. Nature. 2017;552(7684):273-277.
39. Du J, Zhou Y, Su X, et al. Sirt5 is a NAD-dependent protein lysine demalonylase and desuccinylase. Science. 2011;334(6057):806-809.
40. Li L, Shi L, Yang S, et al. SIRT7 is a histone desuccinylase that functionally links to chromatin compaction and genome stability. Nat Commun. 2016;7:12235.
41. An X, Schulz VP, Li J, et al. Global transcriptome analyses of human and murine terminal erythroid differentiation. Blood. 2014;123(22):3466-3477.
42. Zhang X, Song B, Carlino MJ, et al. An immunophenotype-coupled transcriptomic atlas of human hematopoietic progenitors. Nat Immunol. 2024;25(4):703-715.
43. Wang F, Wang K, Xu W, et al. SIRT5 Desuccinylates and Activates Pyruvate Kinase M2 to Block Macrophage IL-1beta Production and to Prevent DSS-Induced Colitis in Mice. Cell Rep. 2017;19(11):2331-2344.
44. Xiao ZP, Lv T, Hou PP, et al. Sirtuin 5-Mediated Lysine Desuccinylation Protects Mitochondrial Metabolism Following Subarachnoid Hemorrhage in Mice. Stroke. 2021;52(12):4043-4053.
45. Liu J, Zhang J, Ginzburg Y, et al. Quantitative analysis of murine terminal erythroid differentiation in vivo: novel method to study normal and disordered erythropoiesis. Blood. 2013;121(8):e43-e49.
46. Ji P, Murata-Hori M, Lodish HF. Formation of mammalian erythrocytes: chromatin condensation and enucleation. Trends Cell Biol. 2011;21(7):409-415.
47. Park J, Chen Y, Tishkoff DX, et al. SIRT5-mediated lysine desuccinylation impacts diverse metabolic pathways. Mol Cell. 2013;50(6):919-930.
48. Bock FJ, Tait SWG. Mitochondria as multifaceted regulators of cell death. Nat Rev Mol Cell Biol. 2020;21(2):85-100.
49. Tehranchi R, Fadeel B, Forsblom AM, et al. Granulocyte colony-stimulating factor inhibits spontaneous cytochrome c release and mitochondria-dependent apoptosis of myelodysplastic syndrome hematopoietic progenitors. Blood. 2003;101(3):1080-1086.
50. Burch JS, Marcero JR, Maschek JA, et al. Glutamine via alpha-ketoglutarate dehydrogenase provides succinyl-CoA for heme synthesis during erythropoiesis. Blood. 2018;132(10):987-998.
51. Furuyama K, Sassa S. Interaction between succinyl CoA synthetase and the heme-biosynthetic enzyme ALAS-E is disrupted in sideroblastic anemia. J Clin Invest. 2000;105(6):757-764.
52. Gu Y, Yang R, Yang Y, et al. IDH1 mutation contributes to myeloid dysplasia in mice by disturbing heme biosynthesis and erythropoiesis. Blood. 2021;137(7):945-958.
53. Yan W, Xie C, Sun S, et al. SUCLG1 restricts POLRMT succinylation to enhance mitochondrial biogenesis and leukemia progression. EMBO J. 2024;43(12):2337-2367.
54. Shen R, Ruan H, Lin S, et al. Lysine succinylation, the metabolic bridge between cancer and immunity. Genes Dis. 2023;10(6):2470-2478.
55. Lian J, Liu W, Hu Q, Zhang X. Succinylation modification: a potential therapeutic target in stroke. Neural Regen Res. 2024;19(4):781-787.
56. Ma W, Sun Y, Yan R, et al. OXCT1 functions as a succinyltransferase, contributing to hepatocellular carcinoma via succinylating LACTB. Mol Cell. 2024;84(3):538-551.e7.
57. Roessler C, Tuting C, Meleshin M, Steegborn C, Schutkowski M. A Novel Continuous

Assay for the Deacylase Sirtuin 5 and Other Deacetylases. J Med Chem. 2015;58(18):7217-7223.
58. Yu J, Sadhukhan S, Noriega LG, et al. Metabolic characterization of a Sirt5 deficient mouse model. Sci Rep. 2013;3:2806.
59. Caielli S, Cardenas J, de Jesus AA, et al. Erythroid mitochondrial retention triggers myeloid-dependent type I interferon in human SLE. Cell. 2021;184(17):4464-4479.e.19.
60. Yang Y, Gibson GE. Succinylation Links Metabolism to Protein Functions. Neurochem Res. 2019;44(10):2346-2359.
61. Sreedhar A, Wiese EK, Hitosugi T. Enzymatic and metabolic regulation of lysine succinylation. Genes Dis. 2020;7(2):166-171.
62. Li Y, Yan JM, Zhou JY, Lu Y-C, Li D-Z. Combination of Hb Heze [beta144(HC1)Lys-->Arg; HBB: c.434A>G] and beta(0)-Thalassemia in a Chinese Patient with beta-Thalassemia Intermedia. Hemoglobin. 2017;41(1):47-49.
63. Henderson SJ, Timbs AT, McCarthy J, et al. Ten Years of Routine alpha- and beta-Globin Gene Sequencing in UK Hemoglobinopathy Referrals Reveals 60 Novel Mutations. Hemoglobin. 2016;40(2):75-84.

Figure legend

Figure 1. Succinylation accumulates during erythropoiesis. (A) Left panel: Illustration of the $CD34^+$ cell culture protocol and Giemsa staining defining each developmental stage of human erythroid differentiation. Right panel: Schematic representation of targeted metabolomics assays for Coenzyme A. (B) Profiling of short-chain CoAs across various stages of human erythroid differentiation using LC-MS/MS (mean ± SEM, n = 5 samples). (C) Isolation of CD34+ cells from each developmental stage of human erythroid differentiation for cell lysis and subsequent detection of global lysine succinylation through western blot, with GAPDH as the loading control. (D) Left panel: Schematic outline of the HUDEP2 cell culture protocol and Giemsa staining defining each developmental stage of human erythroid differentiation. Right panel: Collection of HUDEP2 cells from different stages of human erythroid differentiation for cell lysis and assessment of global lysine succinylation by western blot, with GAPDH as the loading control. Quantitative analysis of protein expression data from three independent experiments. Immunofluorescence analysis depicting overall lysine succinylation levels during human erythroid differentiation at each developmental stage in CD34+ cells (E) and HUDEP2 cells (G) (Scale bars, 10μm). Separation of nuclear and cytosolic fractions from each human erythroid differentiation stage in CD34+ cells (F) and HUDEP2 cells (H) to determine succinylation levels between these fractions, with confirmation of fraction purity using specific markers. Statistical analysis of the data was from three independent experiments, and the bar plot represents the mean ± SD of triplicate samples. *P< .05, **P< .01 versus control based on Student's t-test.

Figure 2. Impact of global lysine succinylation on human terminal erythroid differentiation. (A) Western blot analysis depicting global lysine succinylation levels in HUDEP2 cells following infection with knockdown of succinyltransferases or overexpression of desuccinylases. (B) Growth curves of erythroid cells at various developmental stages, determined by manual cell counting. (C) Left panel: Flow cytometry plots showing gating of apoptosis cells assessed via annexin V/PI staining. Right panel: Cell apoptosis proportions during erythroid differentiation in HUDEP2 cells. (D) Left panel: Flow cytometry plots

showing gating of S-phase cells assessed via BrdU/PI staining. Right panel: Results of cell-cycle distribution obtained through BrdU assay during erythroid differentiation in HUDEP2 cells. (E) Left panel: Flow cytometry plots showing gating of erythroid cells assessed via CD235a+ (GPA) and CD71 staining. Right panel: Proportions of GPA and CD71- cells during erythroid differentiation in HUDEP2 cells. Statistical analysis is derived from three independent experiments, and the bar plot represents the mean ± SD of triplicate samples. Significance levels are denoted as *P< .05, **P< .01, versus control, based on Student's t-test.

Figure 3. Overexpression of SIRT5 inhibits erythroid development in vivo. (A) Immunoblot analysis detecting indicated global lysine succinylation levels in BM cells of control and OV-SIRT5 mice (n = 3). (B) Peripheral blood count analysis in control and OV-SIRT5 mice (n = 5). RBC: red blood cells; HGB: hemoglobin; WBC: white blood cells. (C) Macroscopic views of the lower limb skeleton and limb BM cell pellets from control and OV-SIRT5 mice. (D) Flow cytometric analysis depicting the percentages of $Ter119^+$ cells in BM cells from control and OV-SIRT5 mice. (E) A representative Vertical section of mouse bone marrow showing expression of Ter119 by immunostaining. (F) Flow cytometric analysis of erythroblasts in BM of control and OVSIRT5 mice. The left panel categorizes erythroblasts into five subpopulations by surface staining for CD44 and Ter119: Ter119medCD44 high proerythroblasts (R1). The bottom panel shows representative plots of CD44 versus FSC of $Ter119^+$ cells with gating of populations R2, R3, R4, R5 (basophilic erythroblasts, polychromatic erythroblasts, orthochromatic erythroblasts, reticulocytes). The right panel illustrates the cell distribution analysis based on the flow cytometry results. The bar plot represents the mean ± SD of sample numbers. *$P < 0.05$, **$P < 0.01$ versus control based on Student's t-test (n = 5).

Figure 4. Succinylome and proteome profiling during erythroid differentiation. (A) Experimental workflow showing the 4D-label-free quantification method for both the proteome and succinylome (with an additional succinylation enrichment step). (B) After screening and mining quantitative data, the combined results from 6 samples on early-stage

and late-stage of erythroid differentiation revealed 5563 common proteins and 3540 quantified succinylated peptides from 939 proteins. (C) The distribution of the succinylome intensity in early or late erythroid differentiation stages. (D) Association analysis between succinylome and proteome intensities using Spearman rank correlation, after transforming the intensities to z-scores. (E) Distribution of the number of succinylation sites per protein among all succinylated proteins. (F) Analysis of subcellular localization of quantifiable succinylated proteins (Nuc: nuclear, Cyto: cytoplasm, Mito: mitochondrion).

Figure 5. Differential analysis of the succinylome between early and late erythroid stages. (A) Volcano plot illustrating 939 succinylated proteins in early and late-stages. Each spot represents a specific succinylated peptide. Red symbols to the left of zero indicate significantly downregulated succinylated peptides, while blue symbols to the right of zero indicate significantly upregulated succinylated peptides in late-stage ($P < 0.05$ & $|\log2(\text{fold change})| \geq 0.5$, Student's two-sided t-test). (B) Distribution of differential succinylation peptides (numbers above the line) and succinylated proteins (numbers below the line) according to subcellular localization. (C, D) GO results of upregulated succinylated proteins and downregulated succinylated proteins. (E) Pathway enrichment analysis of the succinylome. The network represents the identified GO and KEGG terms (nodes) and the relationship between them (edges) based on the similarity of associated genes/proteins. The edge weight reflects the similarity between terms.

Figure 6. Integrated analysis of proteome and succinylome. (A) Changes in metabolism-related succinylated proteins in the proteome and succinylome. For each protein, changes in proteome were shown on the left and changes in succinylation were shown on the right. (B) Comparison of the proteome and succinylome changes. Gray dots indicate statistically insignificant results ($P > 0.05$). Blue dots indicate proteins with significantly upregulated succinylation levels but no change in protein levels ($P < 0.05$). Spearman's correlation was calculated to determine the correlation between changes in the succinylome and proteome. (C) Heatmap showing the fold change of each succinylated site for the top 10 highly succinylated proteins in both the proteome and succinylome. Each square corresponds

to a succinylation site.

Figure 7. The CUT&Tag analysis of H3K79Ksu mediated by KAT2A in CD34^{+} cells. (A) Detection of KAT2A protein level and succinylation level with histone H3 at various stages of erythroid differentiation by western blot. GAPDH was used as a loading control. (B) Co-immunoprecipitation (Co-IP) experiment with a KAT2A antibody followed by detection of precipitated proteins using a histone H3 antibody. (C) Western blot showing KAT2A, H3K79 succinylation, and H3 expression in erythroblasts infected with control shRNA or KAT2A shRNA. β-ACTIN was used as a loading control. (D) The peak signal of H3K79Ksu with knocking down KAT2A and control. (E) Representative erythroid genes showing the CUT&Tag signal of H3K79Ksu after KAT2A knockdown. (F). The GO annotation of the affected peaks located in promoter regions. (G) Chromatin immunoprecipitation-PCR assay (ChIP-PCR) results for Succ-H3K79 binding to the FOXO3, CLTA-1, HDAC6, XPO7, and HNRNPU promoter regions. ChIP-PCR was performed using Succ-H3K79 and control IgG antibodies in HUDEP2 cells infected with lentivirus containing control shRNA or KAT2A shRNA.

Figure 8. Altered succinylation of cytochrome C (CYSC) impairs erythroid differentiation. (A) Immunoprecipitation of succinylated proteins using pan-Ksu antibody after transfection of flag-tagged vector, flag-WT-CYCS, or its mutants in HUDEP2 cells with shCYCS. (B-E) Transfection of flag-tagged vector, flag-WT-CYCS, or its mutants into HUDEP2 cells with shCYCS, along with control shRNA and flag-tagged vector co-transfected cells as control. Cell growth curves determined by manual cell counting of HUDEP2 cells (B). Representative images of flow cytometry analysis of apoptosis by annexin V/PI staining in HUDEP2 cells (C). Cell-cycle distribution results of BrdU assay from the above HUDEP2 cells (D). Representative images of flow cytometry analysis of GPA and CD71 expression in HUDEP2 cells (E). (F) Representative flow cytometry analysis of mitochondrial membrane potential using JC-1 staining. (G) The Schematic diagram of this study. Statistical analysis of the data was from three independent experiments, and the bar plot represents the mean ± SD of triplicate samples. *P < .05, **P < .01, ***P < .001, ****P

<0.0001 versus control based on Student’s t-test.

Fig. 1

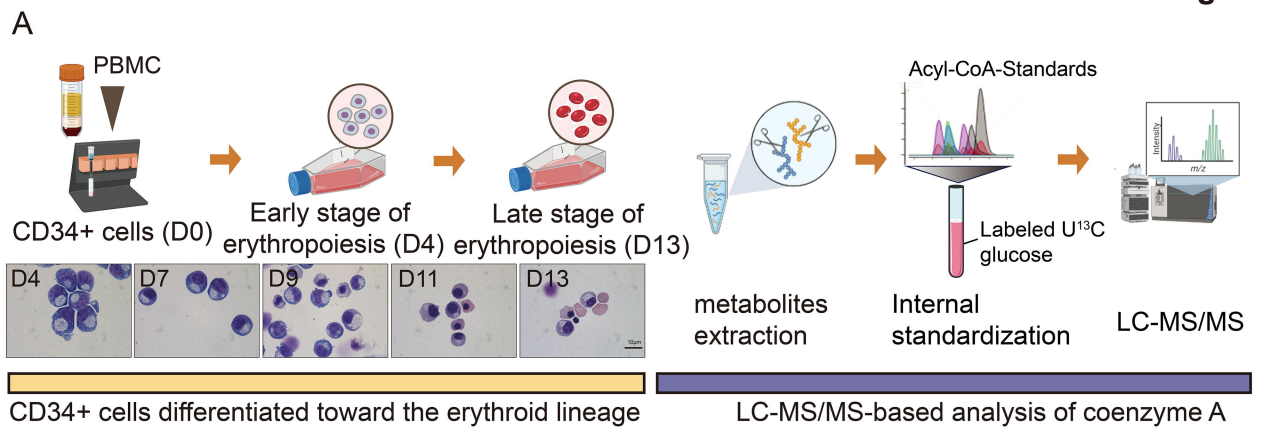
A
PBMC
CD34+ cells (D0)
Early stage of erythropoiesis (D4)
Late stage of erythropoiesis (D13)
D4
D7
D9
D11
D13
Acyl-CoA-Standards
Labeled U13C glucose
metabolites extraction
Internal standardization
LC-MS/MS
CD34+ cells differentiated toward the erythroid lineage
LC-MS/MS-based analysis of coenzyme A

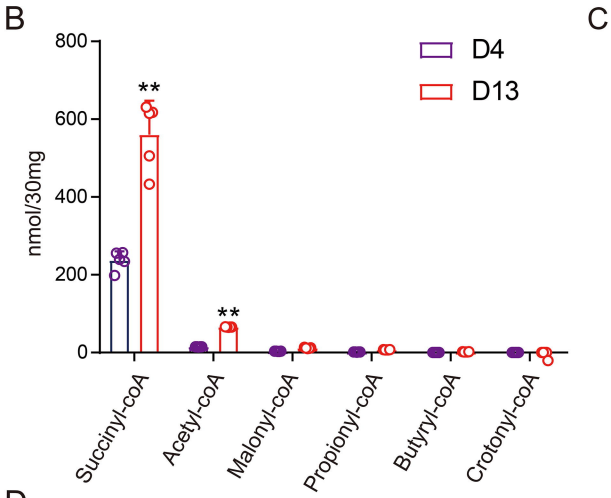
B
D4
D13
nmol/30mg
800
600
400
200
0
**
Succinyl-coA
Acetyl-coA
Malonyl-coA
Propionyl-coA
Butyryl-coA
Crotonyl-coA

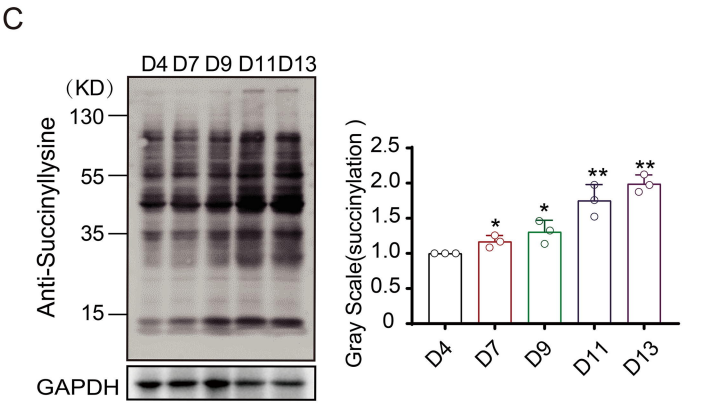
C
D4 D7 D9 D11D13
(KD)
130
55
35
15
Anti-Succinyllysine
GAPDH
Gray Scale(succinylation)
2.5
2.0
1.5
1.0
0.5
0
*
**
D4
D7
D9
D11
D13

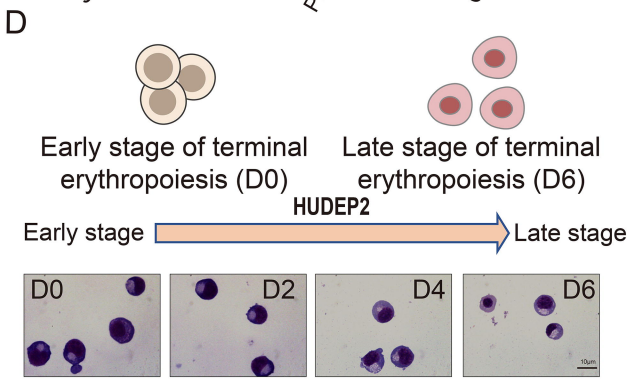
D
Early stage of terminal erythropoiesis (D0)
Late stage of terminal erythropoiesis (D6)
HUDEP2
Early stage
Late stage
D0
D2
D4
D6

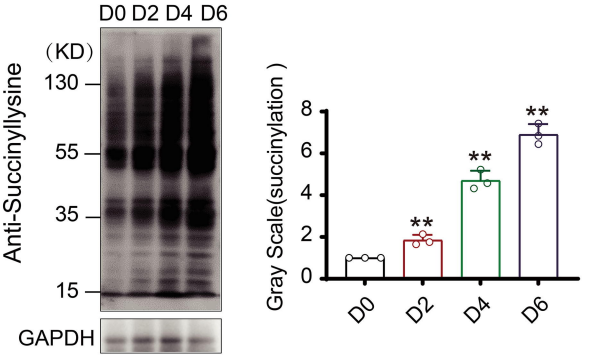
D0 D2 D4 D6
(KD)
130
55
35
15
Anti-Succinyllysine
GAPDH
Gray Scale(succinylation)
8
6
4
2
0
**
D0
D2
D4
D6

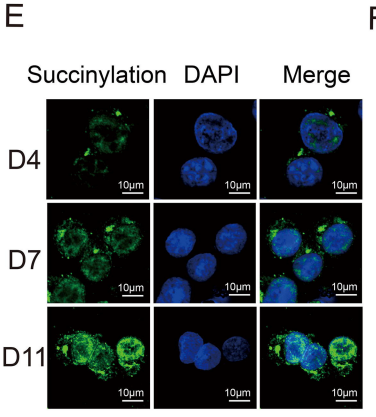
E
Succinylation
DAPI
Merge
D4
D7
D11
10μm

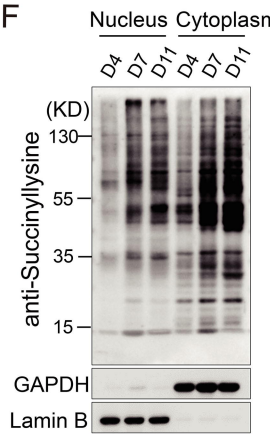
F
Nucleus
Cytoplasm
D4
D7
D11
(KD)
130
55
35
15
anti-Succinyllysine
GAPDH
Lamin B

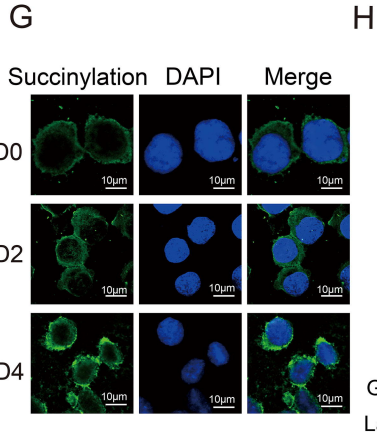
G
Succinylation
DAPI
Merge
D0
D2
D4
10μm

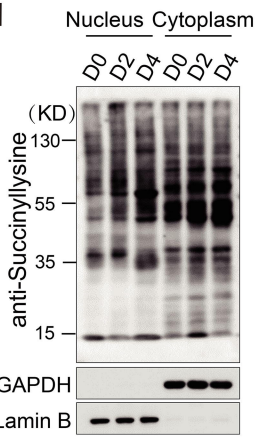
H
Nucleus
Cytoplasm
D0
D2
D4
(KD)
130
55
35
15
anti-Succinyllysine
GAPDH
Lamin B

Fig. 2

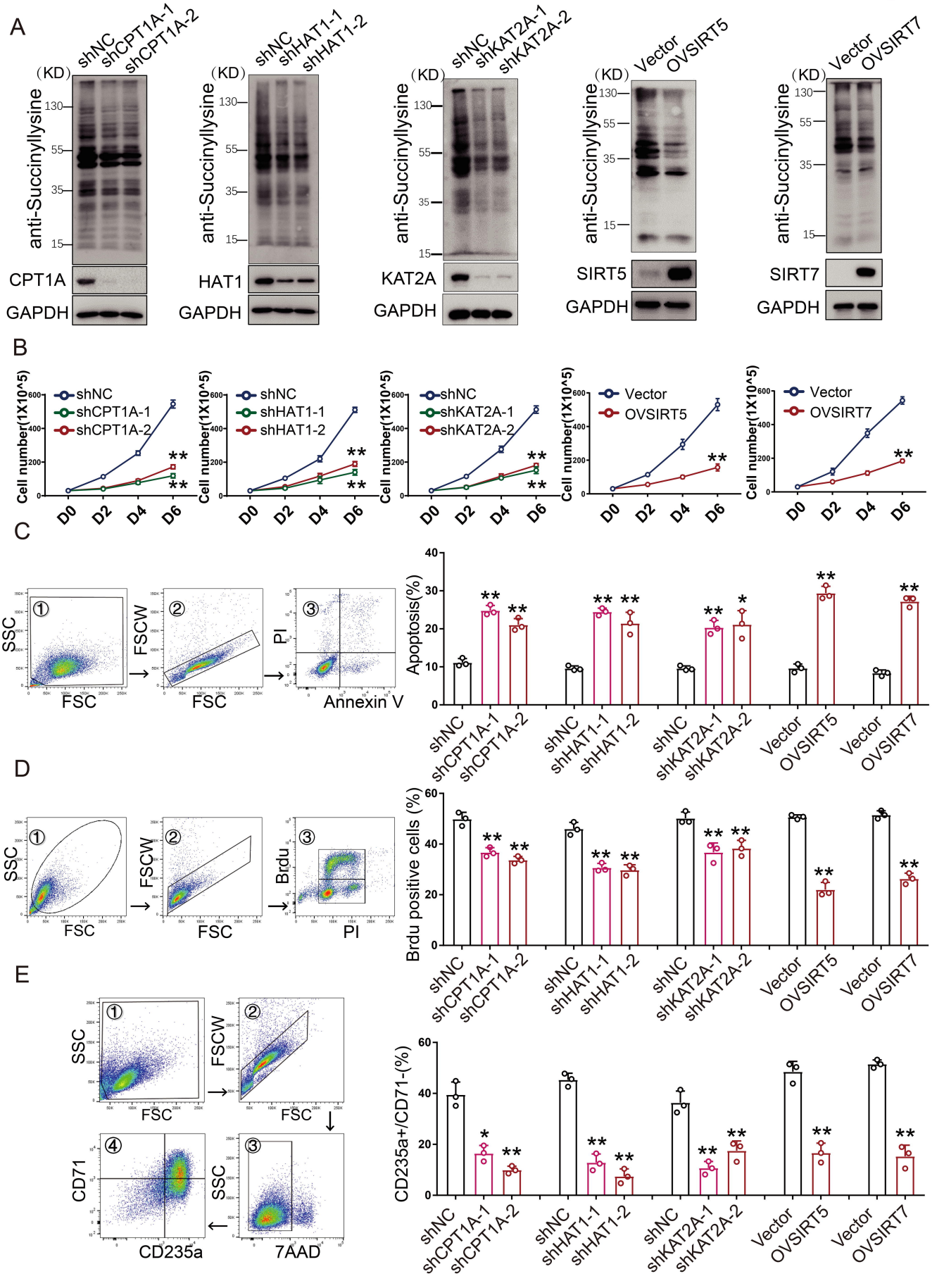
A
shNC
shCPT1A-1
shCPT1A-2
shHAT1-1
shHAT1-2
shKAT2A-1
shKAT2A-2
Vector
OVSIRT5
OVSIRT7
(KD)
anti-Succinyllysine
CPT1A
HAT1
KAT2A
SIRT5
SIRT7
GAPDH
B
Cell number(1X10^5)
D0
D2
D4
D6
C
SSC
FSC
FSCW
PI
Annexin V
Apoptosis(%)
D
Brdu
Brdu positive cells (%)
E
CD71
CD235a
7AAD
CD235a+/CD71-(%)

Fig. 3

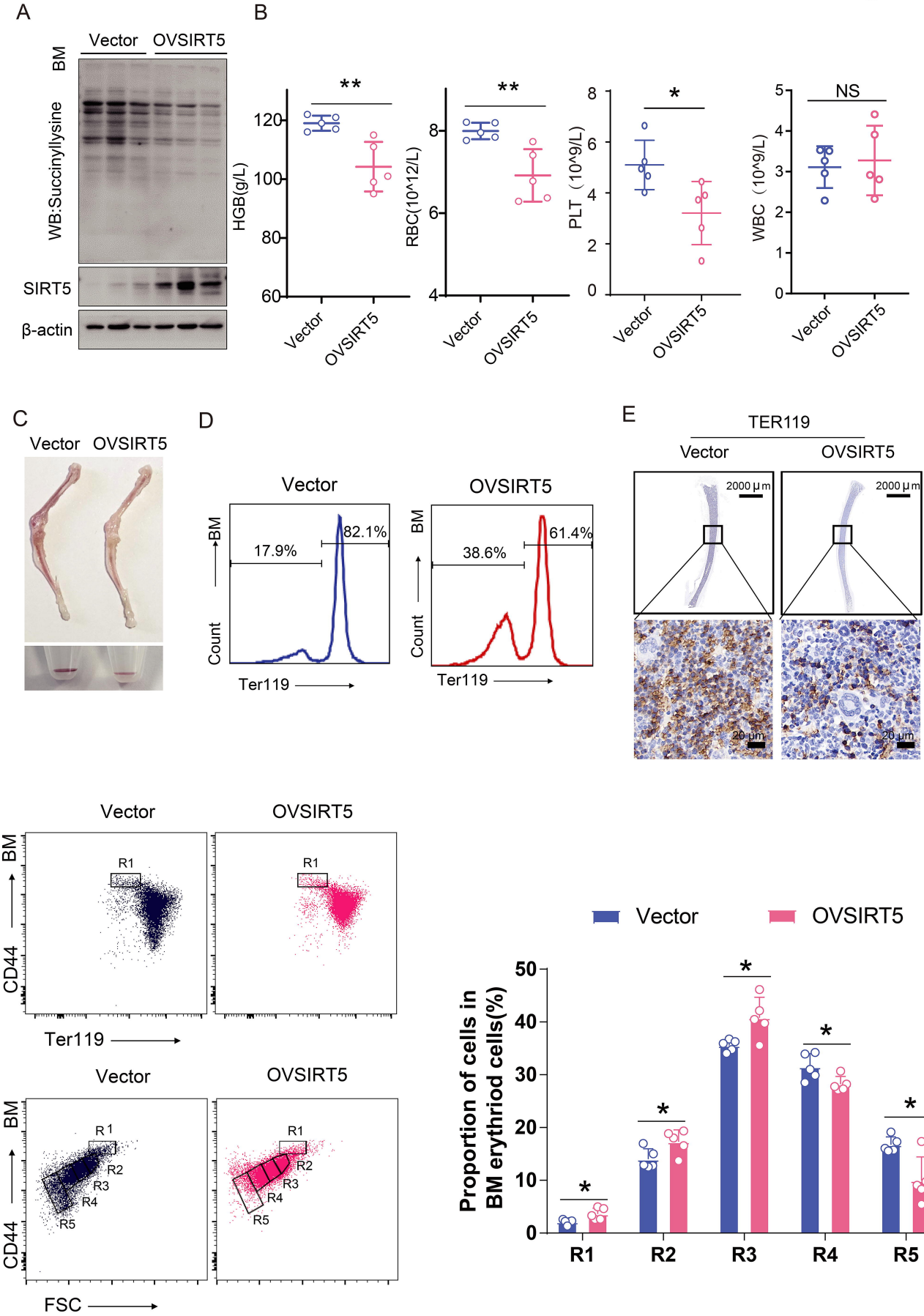
A
Vector
OVSIRT5
BM
WB:Succinyllysine
SIRT5
β-actin
B
HGB(g/L)
RBC(10^12/L)
PLT（10^9/L)
WBC（10^9/L)
**
**
*
NS
Vector
OVSIRT5
C
Vector
OVSIRT5
D
Vector
OVSIRT5
BM
Count
17.9%
82.1%
38.6%
61.4%
Ter119
E
TER119
Vector
OVSIRT5
2000 μm
20 μm
F
Vector
OVSIRT5
BM
CD44
Ter119
R1
R2
R3
R4
R5
FSC
Proportion of cells in BM erythriod cells(%)
R1
R2
R3
R4
R5

Fig. 4

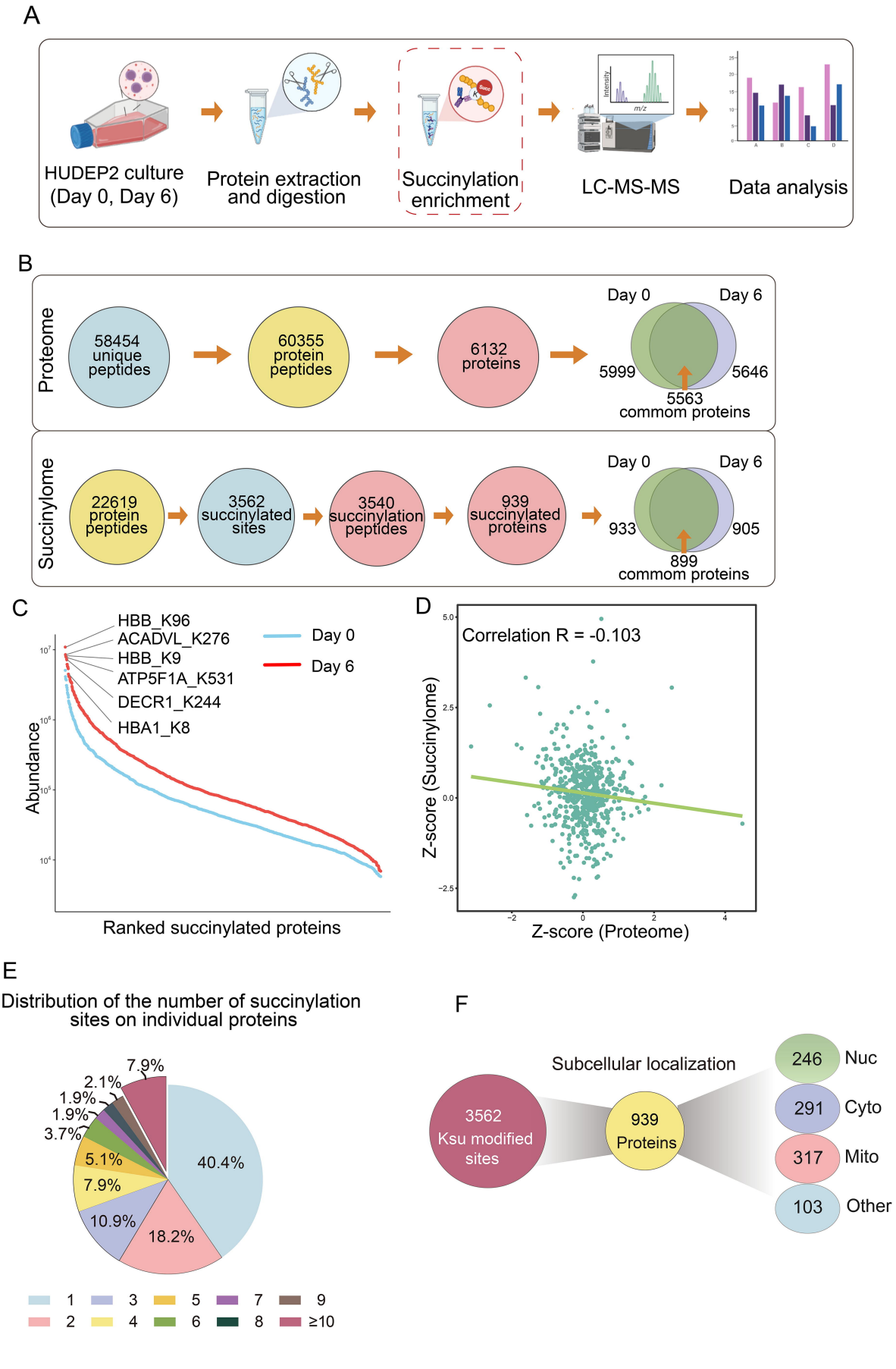
A
HUDEP2 culture (Day 0, Day 6)
Protein extraction and digestion
Succinylation enrichment
LC-MS-MS
Data analysis
B
Proteome
58454 unique peptides
60355 protein peptides
6132 proteins
Day 0
Day 6
5999
5646
5563
commom proteins
Succinylome
22619 protein peptides
3562 succinylated sites
3540 succinylation peptides
939 succinylated proteins
Day 0
Day 6
933
905
899
commom proteins
C
HBB_K96
ACADVL_K276
HBB_K9
ATP5F1A_K531
DECR1_K244
HBA1_K8
Day 0
Day 6
Abundance
Ranked succinylated proteins
D
Correlation R = -0.103
Z-score (Succinylome)
Z-score (Proteome)
E
Distribution of the number of succinylation sites on individual proteins
7.9%
2.1%
1.9%
1.9%
3.7%
5.1%
7.9%
10.9%
18.2%
40.4%
1
2
3
4
5
6
7
8
9
≥10
F
Subcellular localization
3562 Ksu modified sites
939 Proteins
246 Nuc
291 Cyto
317 Mito
103 Other

Fig. 5

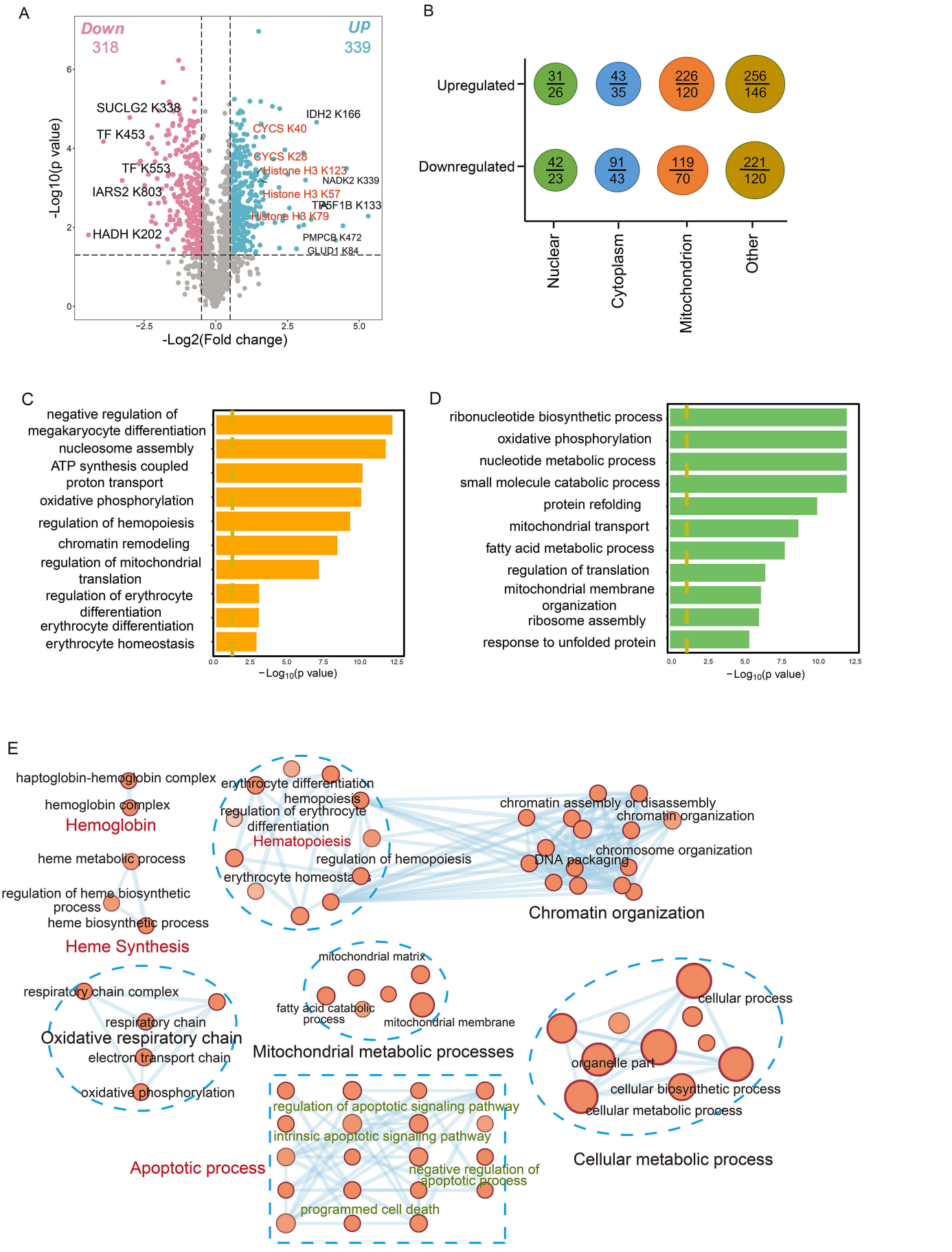
A
Down
318
UP
339
SUCLG2 K338
TF K453
TF K553
IARS2 K803
HADH K202
IDH2 K166
CYCS K40
CYCS K28
Histone H3 K123
NADK2 K339
Histone H3 K57
TPA5F1B K133
Histone H3 K79
PMPCB K472
GLUD1 K84
-Log10(p value)
-Log2(Fold change)
B
Upregulated
Downregulated
31/26
43/35
226/120
256/146
42/23
91/43
119/70
221/120
Nuclear
Cytoplasm
Mitochondrion
Other
C
negative regulation of megakaryocyte differentiation
nucleosome assembly
ATP synthesis coupled proton transport
oxidative phosphorylation
regulation of hemopoiesis
chromatin remodeling
regulation of mitochondrial translation
regulation of erythrocyte differentiation
erythrocyte differentiation
erythrocyte homeostasis
−Log10(p value)
D
ribonucleotide biosynthetic process
oxidative phosphorylation
nucleotide metabolic process
small molecule catabolic process
protein refolding
mitochondrial transport
fatty acid metabolic process
regulation of translation
mitochondrial membrane organization
ribosome assembly
response to unfolded protein
−Log10(p value)
E
haptoglobin-hemoglobin complex
hemoglobin complex
Hemoglobin
heme metabolic process
regulation of heme biosynthetic process
heme biosynthetic process
Heme Synthesis
erythrocyte differentiation
hemopoiesis
regulation of erythrocyte differentiation
Hematopoiesis
regulation of hemopoiesis
erythrocyte homeostasis
chromatin assembly or disassembly
chromatin organization
chromosome organization
DNA packaging
Chromatin organization
respiratory chain complex
respiratory chain
Oxidative respiratory chain
electron transport chain
oxidative phosphorylation
mitochondrial matrix
fatty acid catabolic process
mitochondrial membrane
Mitochondrial metabolic processes
cellular process
organelle part
cellular biosynthetic process
cellular metabolic process
Cellular metabolic process
regulation of apoptotic signaling pathway
intrinsic apoptotic signaling pathway
Apoptotic process
negative regulation of apoptotic process
programmed cell death

A

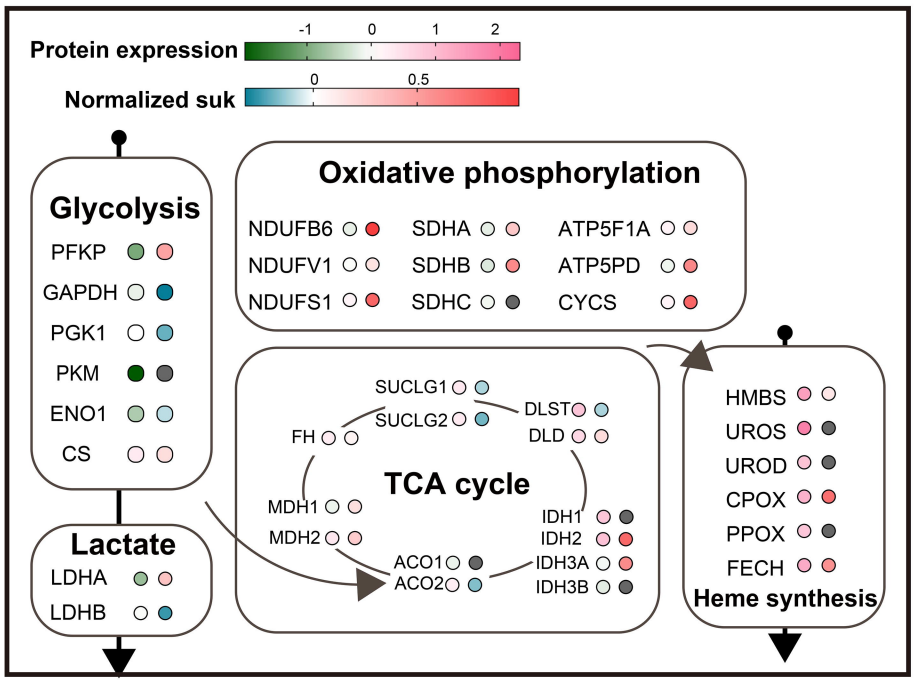
Protein expression
-1
0
1
2
Normalized suk
0
0.5
Glycolysis
PFKP
GAPDH
PGK1
PKM
ENO1
CS
Lactate
LDHA
LDHB
Oxidative phosphorylation
NDUFB6
NDUFV1
NDUFS1
SDHA
SDHB
SDHC
ATP5F1A
ATP5PD
CYCS
TCA cycle
SUCLG1
SUCLG2
FH
DLST
DLD
MDH1
MDH2
IDH1
IDH2
ACO1
ACO2
IDH3A
IDH3B
HMBS
UROS
UROD
CPOX
PPOX
FECH
Heme synthesis

B

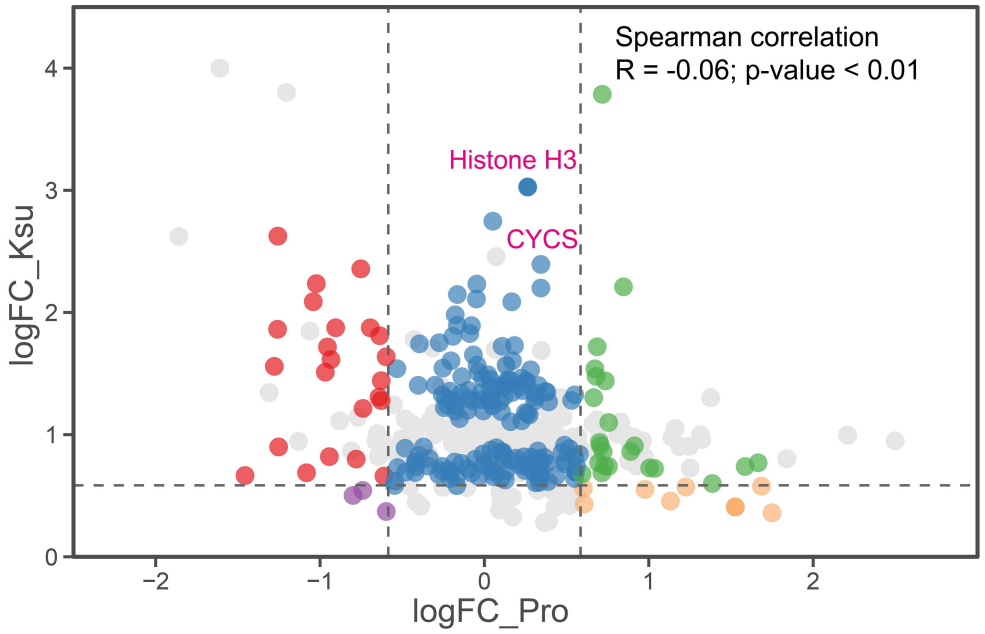
Spearman correlation
R = -0.06; p-value < 0.01
Histone H3
CYCS
logFC_Ksu
logFC_Pro
4
3
2
1
0
−2
−1
0
1
2

C

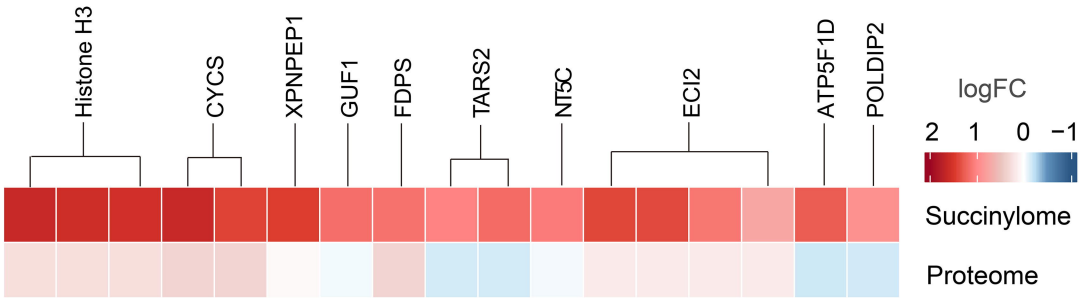
Histone H3
CYCS
XPNPEP1
GUF1
FDPS
TARS2
NT5C
ECI2
ATP5F1D
POLDIP2
logFC
2
1
0
−1
Succinylome
Proteome

Fig. 7

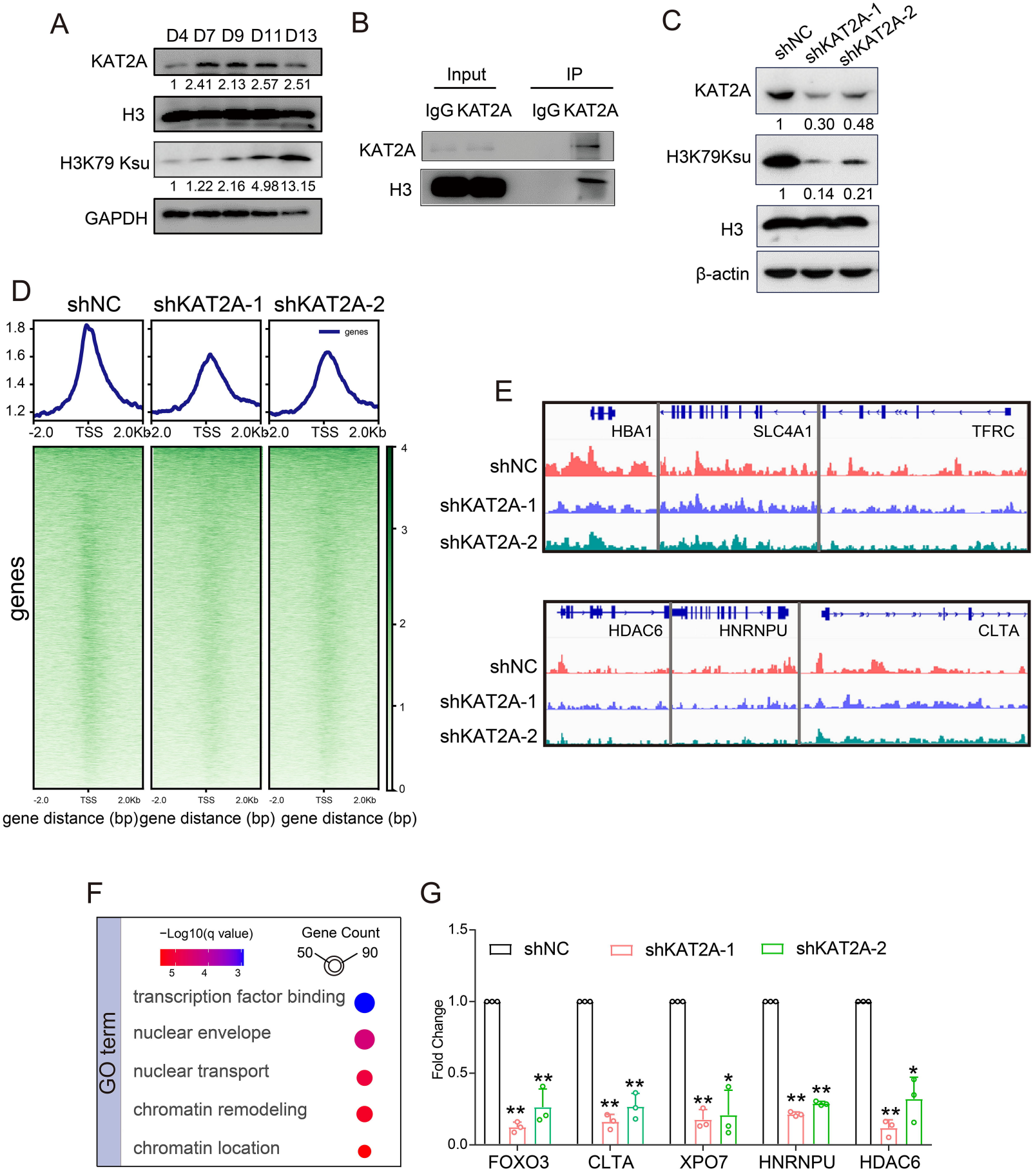
A
D4 D7 D9 D11 D13
KAT2A
1 2.41 2.13 2.57 2.51
H3
H3K79 Ksu
1 1.22 2.16 4.98 13.15
GAPDH
B
Input
IP
IgG KAT2A
IgG KAT2A
KAT2A
H3
C
shNC
shKAT2A-1
shKAT2A-2
KAT2A
1 0.30 0.48
H3K79Ksu
1 0.14 0.21
H3
β-actin
D
shNC
shKAT2A-1
shKAT2A-2
genes
1.8
1.6
1.4
1.2
-2.0 TSS 2.0Kb
4
3
2
1
0
genes
gene distance (bp)
E
HBA1
SLC4A1
TFRC
shNC
shKAT2A-1
shKAT2A-2
HDAC6
HNRNPU
CLTA
F
−Log10(q value)
5 4 3
Gene Count
50 90
GO term
transcription factor binding
nuclear envelope
nuclear transport
chromatin remodeling
chromatin location
G
shNC
shKAT2A-1
shKAT2A-2
Fold Change
1.5
1.0
0.5
0.0
FOXO3
CLTA
XPO7
HNRNPU
HDAC6

Fig. 8

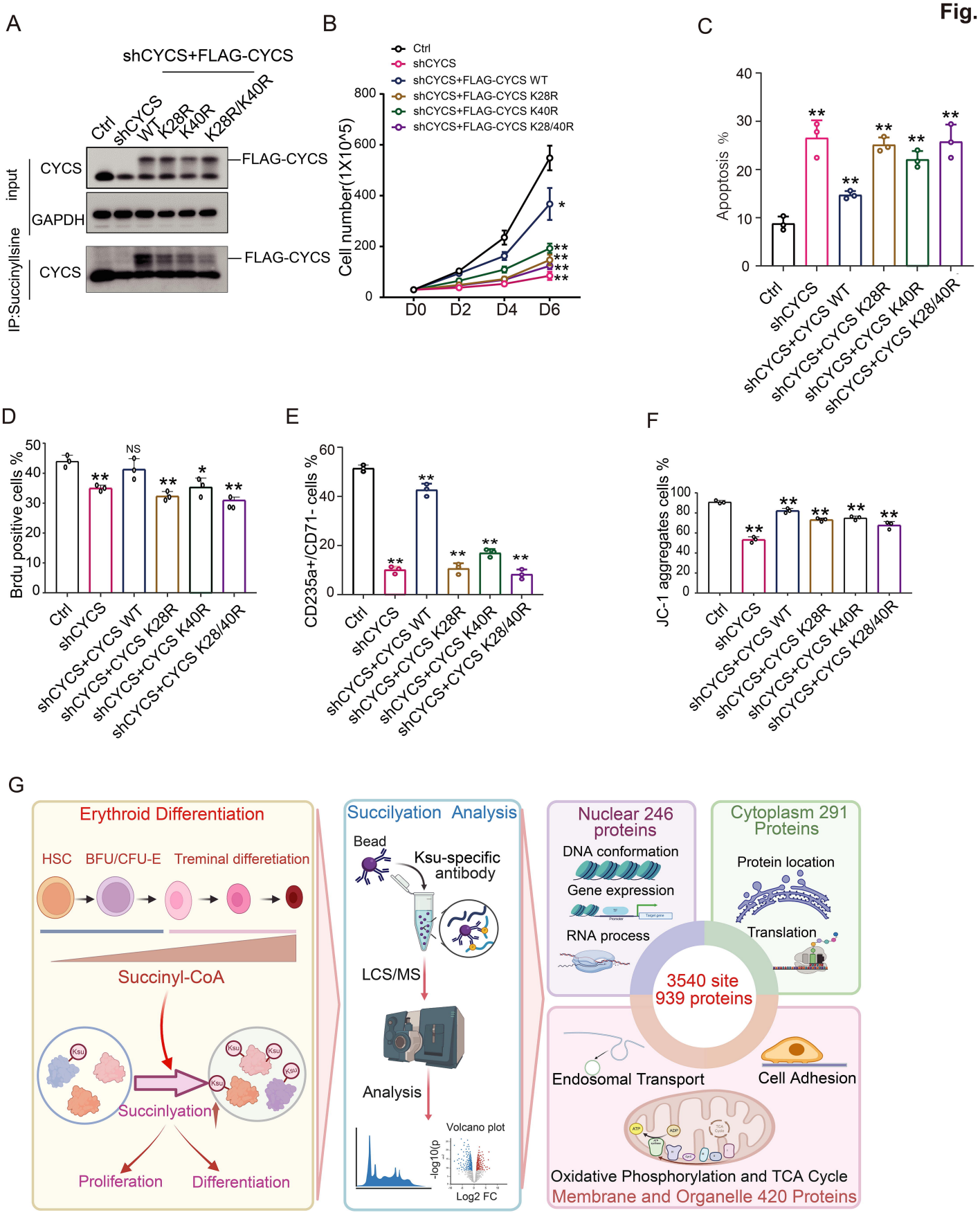
A
shCYCS+FLAG-CYCS
Ctrl
shCYCS
WT
K28R
K40R
K28R/K40R
input
CYCS
FLAG-CYCS
GAPDH
IP:Succinyllsine
CYCS
FLAG-CYCS
B
Ctrl
shCYCS
shCYCS+FLAG-CYCS WT
shCYCS+FLAG-CYCS K28R
shCYCS+FLAG-CYCS K40R
shCYCS+FLAG-CYCS K28/40R
Cell number(1X10^5)
D0
D2
D4
D6
C
Apoptosis %
D
Brdu positive cells %
NS
E
CD235a+/CD71- cells %
F
JC-1 aggregates cells %
G
Erythroid Differentiation
HSC
BFU/CFU-E
Treminal differetiation
Succinyl-CoA
Succinlyation
Proliferation
Differentiation
Succilyation Analysis
Bead
Ksu-specific antibody
LCS/MS
Analysis
Volcano plot
-log10(p
Log2 FC
Nuclear 246 proteins
DNA conformation
Gene expression
RNA process
Cytoplasm 291 Proteins
Protein location
Translation
3540 site
939 proteins
Endosomal Transport
Cell Adhesion
Oxidative Phosphorylation and TCA Cycle
Membrane and Organelle 420 Proteins

Supplemental Methods

$CD34^+$ Cell culture and manipulation

$CD34^+$ cells were purified from peripheral blood mononuclear cells (PMBC) by positive selection with the magnetic-activated cell sorting system (Miltenyi Biotec), according to the manufacturer's instructions. The cell culture procedure was divided into three phases. The cells were cultured in Iscove's modified Dulbecco's medium (IMDM, Life Technologies) containing 200 g/ml human holo-transferrin (sigma-Aldrich), 2% human AB plasma, 10 g/ml insulin (sigma-Aldrich), 3% fetal bovine serum (Gibco FBS, thermofisher), 3 IU/ml heparin (qilu-pharma), and 1% penicillin/streptomycin (Thermofisher) on day 0– day 6, $CD34^+$ cells at a concentration of 10^5/ml were supplemented with 1 ng/ml interleukin 3 (IL-3), 10 ng/ml stem cell factor (SCF, STEMCELL Technologies), and 3 IU/ml EPO. On day 7– day 11, the cells were supplemented with 1 IU/ml EPO and 10 ng/ml SCF alone. day 11–14, the cell concentration was adjusted to 10^6/ml on day 11 and to 5×10^6/ml on day 14. The cells were maintained at 37℃ at the presence of 5% CO_2, and were split into fresh culture medium every 2 days.

HUDEP2 cells towards erythroid lineage

Begin culture of HUDEP2 cells from frozen stock by plating in HUDEP2 expansion media at 100,000 cells/mL. The HUDEP2 cells typically double every 24–36 h. Perform media changes every 3–4 days, while ensuring that the cell density remains below 800,000 cells/mL. The cells were cultured with expansion medium: StemSpa Serum-Free Expansion Medium (SFEM,Stemcell Technologies), 2% PenicillinStreptomycin solution (10000 U/mL stock), 50 ng/mL recombinant human stem cell factor (SCF), 3 IU/mL EPO, 0.4μg/mL dexamethasone, 1 μg/mL doxycycline. Culturing HUDEP2 Cells for Erythroid Differentiation Phase, Transfer the cells from expansion medium, then the cells were cultured in Iscove's modified Dulbecco's medium (IMDM), 1% L-glutamine (this is in addition to the L-glutamine present in IMDM), 2% PenicillinStreptomycin solution (10,000U/mL stock concentration), 330μg/mL human holo-transferrin, 10μg/mL recombinant human insulin solution, 2 IU/mL heparin, 5% inactivated human plasma, 3 IU/mL EPO.

Cytospin preparation

A total of 1×105 cells in 100 μL DPBS were spun for 5 minutes at 400 rpm onto glass slides using the cytospin apparatus. After airdrying for 1 minute, slides were stained with Giemsa staining solution (Sigma, Darmstadt, Germany) according to manufacturer's instructions. Stained cells were viewed, and images were acquired with an Olympus BX51 microscope and QCapture Pro 6.0 (Tokyo, Japan).

Plasmid construction

Primers of two human shRNA were annealed, followed by subcloning into pLKO.1 vectors at AgeI and EcoRI restriction enzyme sites. KAT2A, CPT1A and HAT1 were amplified and cloned into MSCV-puro at AgeI and EcoRI restriction enzyme sites. Cycs overexpression plasmid was cloned into pcl20-N-2*flag-Blasticidin at EcoRI restriction enzyme sites.

Virus preparation

For lentivirus production, pLKO.1 shRNA or pcl20-N-2*flag-Blasticidin together with package plasmids pMDG.2 and PSPAX2 were transfected into 293T cells by PEI (polysciences). For retrovirus production, MSCV vector combined with PECO package vector, were transfected into 293T cells by PEI. The supernatant medium containing virus was collected after 48 and 72 h. The virus medium was filtered by 0.45 μM filter (Millipore) before use.

Cell infection

Cells were mixed with virus medium, 4 μg/ml polybrene was added and cells were spinoculated for 3 h at 32 °C. In the following day, spinoculation was repeated. Then 1 μg/ml puromycin (Solarbio) and 20 μg/ml Blasticidin (Beyotime) were added to select the positive cells.

Western blot analysis

Protein extracts were subject to polyacrylamide gels (Bio-Rad), transferred to a NC membrane, and incubated in blocking buffer (5% non-fat milk in PBST). Antibody staining was visualized using the Bio-rad Imaging System. For western blotting, the primary antibody was diluted to 1:500 by blocking buffer with a final concentration of 2 μg/mL. The secondary antibody (goat anti-rabbit or anti-mouse IgG [H+L] with HRP (abbkine) was diluted to 1:5000 by blocking buffer with a final concentration of 0.4 μg/mL. The SuperSignal™ West Femto Maximum Sensitivity Substrate (Thermo Fisher Scientific) was used for antibody signal detection.

Co-immunoprecipitation

Total cell lysates were prepared from HUDEP2 cells using RIPA IP buffer (Beyotime). the cell lysate was precleared with Pierce Protein A/G magnetic beads (Bimake) for 30min then incubated with the antibody overnight. This was followed by incubation for 2 h with fresh Protein A/G magnetic beads. The beads were then washed three times with IP buffer, and 2× SDS-PAGE sample buffer was added. Samples were boiled for 10 min then centrifuged, and the supernatants were subjected to Western blot analysis. Immunoprecipitation was conducted using an anti-KAT2A antibody.

Immunofluorescence

Sections were permeabilized with 0.1% Triton X-100 in PBS for 15 min at room temperature, treated with 3% BSA and 3% goat serum, 0.1% Triton, and 0.05% Tween-20 in PBS for 1 h, and then incubated with anti-succinyllysine antibody overnight at 4°C. Sections were then washed extensively, incubated with the secondary antibody for 2 h at room temperature, mounted on glass slides, and visualized with a confocal laser scanning microscope (OLYMPUS).

Chromatin Immunoprecipitation (ChIP)-PCR

ChIP was performed with anti-succ-H3K79 antibody (PTM BIO) in HUDEP2 cells using Chromatin Immunoprecipitation (ChIP) Kit (9003S, Cell Signaling Technology, CST) according to the manufacturer's protocol. Quantitative PCR analysis was performed on the immunoprecipitated DNA using SYBR qRT-PCR analysis Master Mix (Vazyme). The PCR primers are listed in supplemental Table 4.

Cleavage Under Targets & Tagmentation (CUT&Tag) assay and sequencing data analysis

$CD34^+$ cells were collected to perform the CUT&Tag assay by using NovoNGS CUT&Tag 4.0 High-Sensitivity Kit (for Illumina®) (Novoprotein, N259-YH01). The library sequencing was performed by Illumina novaseq 6000 platform (Haplox Genomics center). FastQC software was used for quality control. The clean reads were aligned to hg38 genome using bowtie2 (v2.3.5.1) with the options (--very-sensitive--end-to-end). Then, the low-quality mapping reads were removed using SAMtools with the option (-q 35). Peak calling was performed by Macs2 (v.2.2.7.1). BW files were visualized using IGV software. Heatmaps were then generated using DeepTools (v.3.5.1) tool. The R package ChIPseeker was used to perform annotation and functional enrichment analysis for differential binding peak between groups.

BrdU assay

The medium was removed from $1x10^6$ cells and replaced with BrdU-labeled solution. After 3 hours incubation at 37°C, the cells were washed twice with PBS and resuspended in 100 μL BD Cytofix/Cytoperm buffer (BD Biosciences), and then incubated on ice for 15-30 minutes until cooling. The cooled cells were washed with 1 mL 1x BD Perm/Wash buffer (BD Biosciences). The cells were centrifuged at 5000 rpm for 5 min and the supernatant was removed. Subsequently, the cells were resuspended in 100 μL BD Cytoperm Permeability Stability Buffer Plus (BD Biosciences) and incubated on ice for 10 min and then washed with 1 mL 1x BD Perm/Wash buffer, centrifuged at 5000 rpm for 5 min and the supernatant removed. Following the up step, the cells were incubated in 100 μL BD Cytofix/Cytoperm buffer on ice for 5 min followed by washing with 1 mL 1x BD Perm/Wash buffer, centrifuged at 5000 rpm for 5 min and the supernatant removed. Immediately, the cells were treated with DNase (300 μg/mL working concentration diluted in DPBS from 6 mg/mL stock solution (Sigma-Aldrich), to expose incorporated BrdU. 100 μL of the diluted DNase (300 μg/mL in DPBS) was used to resuspend the cells and incubated at 37°C in the dark for 1 hour. After this, the cells were washed with 1 mL 1x BD Perm/Wash buffer, centrifuged at 5000 rpm for 5 min and the supernatant removed. the cell pellet was resuspended in 50 μL 1x BD Perm/Wash buffer with the addition of BrdU antibody (ThermoFisher) at 5 μL per 10^6 cells. Then the cells were incubated for 20 min at room temperature and washed with 1 mL 1x BD Perm/Wash buffer, centrifuged at 5000 rpm for 5 min and the supernatant removed. Finally, the cells were stained with 100 μL FACS buffer containing 1 μL of 1 mg/mL DAPI (BioSharp) and incubated in the

dark for 30 min. The stained cells were then used for flow cytometric analysis.

LC-MS/MS analysis and database search

The peptides were separated using a NanoElute ultra-high-performance liquid chromatography system. Once separated, the peptides were ionized by injection into a Capillary ion source and analyzed using the timsTOF Pro mass spectrometer. The ion source voltage was set at 1.65 kV, and high-resolution TOF was used to detect and analyze both the peptide precursor ions and their fragment ions. The secondary mass spectrometry scan range was set to 400-1500 m/z. Parallel accumulation serial fragmentation (PASEF) mode was used for data acquisition, where 10 PASEF mode scans were performed to collect the secondary spectra of precursor ions with charges between 0-5 after collecting one primary mass spectrum. The dynamic exclusion time for tandem mass spectrometry scanning was set to 30 seconds to avoid repeat scans of precursor ions. Protein identification was performed using MaxQuant software (v1.6.15.0), and a total of 20,395 Homo sapiens sequences were downloaded from the UniProtKB database (Release 2021-01) for database searching. Carbamidomethyl (C) was set as a fixed modification for cysteine alkylation, and variable modifications included oxidation of methionine and acetylation of protein N-termini. For succinylome, succinylated lysine residue was added as a variable modification. The false discovery rate (FDR) threshold for protein, peptide, and modification site was set to 1%. The peptide mass tolerance and fragment mass tolerance were set to 10 ppm and 0.02 Da, respectively. The probability for site localization was set to >0.75.

LC-MS/MS analysis and database search

The peptides were separated using a NanoElute ultra-high-performance liquid chromatography system. Once separated, the peptides were ionized by injection into a Capillary ion source and analyzed using the timsTOF Pro mass spectrometer. The ion source voltage was set at 1.65 kV, and high-resolution TOF was used to detect and analyze both the peptide precursor ions and their fragment ions. The secondary mass spectrometry scan range was set to 400-1500 m/z. Parallel accumulation serial fragmentation (PASEF) mode was used for data acquisition, where 10 PASEF mode scans were performed to collect the secondary spectra of precursor ions with

charges between 0-5 after collecting one primary mass spectrum. The dynamic exclusion time for tandem mass spectrometry scanning was set to 30 seconds to avoid repeat scans of precursor ions. Protein identification was performed using MaxQuant software (v1.6.15.0), and a total of 20,395 Homo sapiens sequences were downloaded from the UniProtKB database (Release 2021-01) for database searching. Carbamidomethyl (C) was set as a fixed modification for cysteine alkylation, and variable modifications included oxidation of methionine and acetylation of protein N-termini. For succinylome, succinylated lysine residue was added as a variable modification. The false discovery rate (FDR) threshold for protein, peptide, and modification site was set to 1%. The peptide mass tolerance and fragment mass tolerance were set to 10 ppm and 0.02 Da, respectively. The probability for site localization was set to >0.75.

Supplemental Tables and Figures

Supplemental Table 1. All antibodies used in this study

Antibodies	**Catolog**	**Company**	**Use**
Anti-Succinyllysine Mouse mAb	PTM-419	PTMBIO	Western blot
Anti-HAT1 Mouse mAb	PTM-5195	PTMBIO	Western blot
Anti-Succinyllysine Rabbit pAb	PTM-401	PTMBIO	IF
Anti-Succinyl-Histone H3 (Lys79) Rabbit pAb	PTM-412	PTMBIO	Western blot, IP and ChIP
SIRT5 Rabbit pAb	A5784	abclonal	Western blot
SIRT7 Rabbit pAb	A0979	abclonal	Western blot
Lamin B1 Rabbit pAb	A1910	abclonal	Western blot
HBB Polyclonal antibody	16216-1-AP	proteintech	Western blot
Cytochrome c Polyclonal antibody	10993-1-AP	proteintech	Western Blot
GCN5L2 (KAT2A) Rabbit mAb #3305	C26A10	Cell Signaling Technology	Western Blot and IP
CPT1A (D3B3) Rabbit mAb #12252	D3B3	Cell Signaling Technology	Western blot
Histone H3 Antibody #9715	9715S	Cell Signaling Technology	Western blot
GAPDH antibody(0411)	sc-47724	Santa Cruz Biotechnology	Western blot
beta Actin antibody (C4)	sc-47778	Santa Cruz Biotechnology	Western blot
Anti-DDDDK(FLAG)-tag antibody	M185-3L	MBL	Western blot
BD Pharmingen™ 7-AAD	559925	BD Biosciences	Flow cytometry
BV421 Mouse Anti-Human CD235a	562938	BD Biosciences	Flow cytometry
BD Pharmingen™ PE Mouse Anti-Human CD71	555537	BD Biosciences	Flow cytometry
BD Pharmingen™ DAPI Solution	564907	BD Biosciences	Flow cytometry
BrdU Monoclonal Antibody (BU20A), FITC	11-5071-42	Invitrogen	Flow cytometry

Abbreviations: IP, immunoprecipitation; ChIP, chromatin immunoprecipitation; IF: immunofluorescence.

Supplemental Table 2. Specific reagents used.

Product name	**Company**	**Catalog #**	**Applications in the present study**
CD34 Microbead kit	miltenyibiotec	130-046-702	Cell separation
IMDM	thermofisher	31980030	Cell Culture
holo-transferrin	sigma-Aldrich	11096-37-0	Cell culture
insulin	sigma-Aldrich	11061-68-0	Cell culture
fetal bovine serum	thermofisher	30044333	Cell culture
heparin	qilu-pharma		Cell culture
penicillin/streptomycin	thermofisher	15140122	Prevent bacterial contamination of cell cultures
stem cell factor	STEMCELL Technologies	78064	Cell culture
EPO	Sinovac Biotech Ltd		Cell culture
StemSpan serum-free medium STEMCELL Technologies	STEMCELL Technologies	09600	Cell Culture
Doxycycline	selleck	S5159	Cell Culture
dexamethasone	selleck	S1322	Cell Culture
HEK293T cells	ATCC® CRL-11268™		Cell culture
DMEM	thermofisher	12430054	Cell Culture
PEI	polysciences	02371-100	non-viral vector carriers
0.45 μM filter	millipore	HAWP04700	Filtered plasma
puromycin	Solarbio	P8230	screening strains
Blasticidin	beyotime	ST018-5ml	screening strains
Pierce Protein A/G magnetic beads	bimake	B23201	Antibody purification and immunoprecipitation
BD Cytofix/Cytoperm buffer	BD Biosciences	51-2090KZ	Brdu cell proliferation assay

1× BD Perm/Wash buffer	BD Biosciences	554723	Brdu cell proliferation assay
BD Cytoperm Perme Stability Buffer Plus	BD Biosciences	51-2356KC	Brdu cell proliferation assay
BrdU(dilution of dnase	sigma-Aldrich	32160405	Brdu cell proliferation assay
DAPI	biosharp	BS097-10mg	Flow cytometry and immunofluorescence.
Chromatin Immunoprecipitation (ChIP) Kit	Cell Signaling Technology	9003S	Detect protein-DNA interactions
BCA assay kit	Thermo Scientific	23225	determination of protein concentration
SuperSignal™ West Pico PLUS	Thermo Scientific	34580	Protein Electrophoresis & Western Blotting
Annexin V-FITC/PI Apoptosis Detection Kit	Vazyme	A211-01	apoptosis assay
NE-PER Nuclear and Cytoplasmic Extraction Reagents	Thermo Scientific	78835	Nuclear and Cytoplasmic Extraction

Supplemental Table 3. Oligonucleoties used in this study.

Name	Sequence (5' to 3')	Type
shKAT2A-1-F	CCGGGCTGAACTTTGTGCAGTACAACTCGAGTTGTAC TGCACAAAGTTCAGCTTTTTG	shRNA
shKAT2A-1-R	AATTCAAAAAGCTGAACTTTGTGCAGTACAACTCGAG TTGTACTGCACAAAGTTCAGC	shRNA
shKAT2A-2-F	CCGGCCACCTGAAGGAGTATCACATCTCGAGATGTGA TACTCCTTCAGGTGGTTTTTG	shRNA
shKAT2A-2-R	AATTCAAAAACCACCTGAAGGAGTATCACATCTCGAG ATGTGATACTCCTTCAGGTGG	shRNA
shHAT1-1-F	CCGGGCTACATGACAGTCTATAATTCTCGAGAATTATA GACTGTCATGTAGCTTTTTG	shRNA
shHAT1-1-R	AATTCAAAAAGCTACATGACAGTCTATAATTCTCGAG AATTATAGACTGTCATGTAGC	shRNA
shHAT1-2-F	CCGGCCGTGTTGAATATGCATCTAACTCGAGTTAGATG CATATTCAACACGGTTTTTG	shRNA
shHAT1-2-R	AATTCAAAAACCGTGTTGAATATGCATCTAACTCGAGT TAGATGCATATTCAACACGG	shRNA
shCPT1A-1-F	CCGGCGTAGCCTTTGGTAAAGGAATCTCGAGATTCCT TTACCAAAGGCTACGTTTTTG	shRNA
shCPT1A-1-R	AATTCAAAAACGTAGCCTTTGGTAAAGGAATCTCGAG ATTCCTTTACCAAAGGCTACG	shRNA
shCPT1A-2-F	CCGGCGATGTTACGACAGGTGGTTTCTCGAGAAACCA CCTGTCGTAACATCGTTTTTG	shRNA
shCPT1A-2-R	AATTCAAAAACGATGTTACGACAGGTGGTTTCTCGAG AAACCACCTGTCGTAACATCG	shRNA
shCYCS-F	CCGGAGGGCAGACTTATGATTAGACTTCGTTAGTAATC TATTAAGTCTGCCCTTTTTTG	shRNA
shCYCS-R	AATTCAAAAAAGGGCAGACTTAATAGCTTATCTCGAG ATAAGCTATTAAGTCTGCCCT	shRNA

Abbreviations: F, forward; R, reverse.

Supplemental Table 4. CHIP-qPCR Primers used in this study.

Name	Sequence (5' to 3')
CHIP-PCR primer for hFOXO3	tttaattcagaaagatgtactcaatatttaattaaagatatgagatctaacgatgtaggcaggctgcgggag cagggagtatgccctgtgtaaggactccattc
CHIP-PCR primer for hHDAC6	tgaatgagagaatgaacgagtggttgaatggggaaatgagtggtagaggaaactggcaactgttgggtt gggggtgtctatggggattgacttctccaactctcttacctctttttcttc
CHIP-PCR primer for hXPO7	tcttctatagcatcaaataaagagacctataaatggttattaggtgaatgttacccaggttctcctcagttcag aagcaattctttctttactgattatt
CHIP-PCR primer for hHNRNPU	actattgttccccaaaggtccttagtaataaaggacttagtaataggaaaactttcttggaagagatacatgc aatatgtcacatatcacagatacacatatacaaa
CHIP-PCR primer for hCTLA	cctagg ctcgagaagc ctgttcggtt ctcagcatgt ttgagtgcttctgggcgcgg gcggagcgag aaagcaagtgtagggtggcaggctccggagccggaagaagcccgttcaattcagcaacttttcattaag catttgctgtgcctttagtccggtctctgaagcaaccgcattggcgcagtttttccagacttataagcttataa gtctgagccgagcacagaactcgttattagaaaaggagggcggaaaaaaataagaatggaaatatcgtt tttgagagatacaaacaaaagtagcaatgcagttcagcatttaagcacttaaggtgtacagagtgttggatt acgaggaggaaggagggagtagggaactcgaaagatgatctaggtctggagaaagaactgccaagc gcggtaggagtttgctatcgttgagcgattgatttacagctaggacttctggagctcttcctctgggaacag ctttggtaggcaatattgcctaagca

Supplemental Table 5. Succinylated proteins only in Day 0

UNIPROT	SYMBOL	GENENAME	sites
O00411	POLRMT	RNA polymerase mitochondrial	K402
O14874	BCKDK	branched chain keto acid dehydrogenase kinase	K184, K233, K89, K192
O43766	LIAS	lipoic acid synthetase	K318
O75879	GATB	glutamyl-tRNA amidotransferase subunit B	K529
P21583	KITLG	KIT ligand	K42
P82921	MRPS21	mitochondrial ribosomal protein S21	K40
Q14197	MRPL58	mitochondrial ribosomal protein L58	K153, K118, K94, K98
Q14644	RASA3	RAS p21 protein activator 3	K15
Q14CZ7	FASTKD3	FAST kinase domains 3	K471, K481
Q1512	PDK3	pyruvate dehydrogenase kinase 3	K278

0			
Q53R41	FASTKD1	FAST kinase domains 1	K785, K482, K360, K478, K236
Q5T5X7	BEND3	BEN domain containing 3	K816, K821, K822, K824
Q6P4F2	FDX2	ferredoxin 2	K184
Q6PML9	SLC30A9	solute carrier family 30 member 9	K487, K223, K234
Q7Z3T8	ZFYVE16	zinc finger FYVE-type containing 16	K435
Q86WA6	BPHL	biphenyl hydrolase like	K126, K257, K191, K271
Q86YH6	PDSS2	decaprenyl diphosphate synthase subunit 2	K285
Q8IVH4	MMAA	metabolism of cobalamin associated A	K88, K323
Q8N8R5	C2orf69	chromosome 2 open reading frame 69	K346
Q8NCN5	PDPR	pyruvate dehydrogenase phosphatase regulatory subunit	K854, K100, K219, K307, K218
Q96C01	FAM136A	family with sequence similarity 136 member A	K18
Q96GC5	MRPL48	mitochondrial ribosomal protein L48	K64
Q96I51	RCC1L	RCC1 like	K209
Q96PE7	MCEE	methylmalonyl-CoA epimerase	K114, K60, K150
Q99595	TIMM17A	translocase of inner mitochondrial membrane 17A	K56
Q9BYN8	MRPS26	mitochondrial ribosomal protein S26	K185
Q9HC36	MRM3	mitochondrial rRNA methyltransferase 3	K251, K167, K153, K136, K122, K237
Q9HD34	LYRM4	LYR motif containing 4	K44, K47
Q9NWS8	RMND1	required for meiotic nuclear division 1 homolog	K240, K249
Q9UGM6	WARS2	tryptophanyl tRNA synthetase 2, mitochondrial	K333, K354, K234, K198
Q9UHN1	POLG2	DNA polymerase gamma 2, accessory subunit	K463, K288
Q9Y2	MRPS1	mitochondrial ribosomal protein S17	K21

R5	7		
Q9Y3D5	MRPS18C	mitochondrial ribosomal protein S18C	K131, K134

Supplemental Table 6. Succinylated proteins only in Day 6

UNIPROT	SYMBOL	GENENAME	sites
P02671	FGA	fibrinogen alpha chain	K202, K89, K476, K148, K157
P02675	FGB	fibrinogen beta chain	K374
P02679	FGG	fibrinogen gamma chain	K231
P78540	ARG2	arginase 2	K229, K241
Q4G176	ACSF3	acyl-CoA synthetase family member 3	K534, K563
Q9HD23	MRS2	magnesium transporter MRS2	K93

Supplemental Table 7. Enrichment analysis of stage-specific Ksu proteins

Enrichment analysis of early-stage specific proteins					
ID	Description	pvalue	p.adjust	qvalue	Count
GO:0140053	mitochondrial gene expression	3.16E-16	1.18E-13	9.69E-14	10
GO:0032543	mitochondrial translation	1.25E-13	2.33E-11	1.91E-11	8
GO:0000959	mitochondrial RNA metabolic process	9.22E-07	0.000115	9.41E-05	4
GO:0070131	positive regulation of mitochondrial translation	1.48E-06	0.000139	0.000114	3
GO:0070129	regulation of mitochondrial translation	6.54E-06	0.000489	0.0004	3
Enrichment analysis of late-stage specific proteins					
ID	Description	pvalue	p.adjust	qvalue	Count
GO:0034116	positive regulation of heterotypic cell-cell adhesion	8.21E-09	1.11E-06	2.32E-07	3
GO:0072378	blood coagulation, fibrin clot formation	8.21E-09	1.11E-06	2.32E-07	3
GO:0072376	protein activation cascade	1.23E-08	1.11E-06	2.32E-07	3
GO:0042730	fibrinolysis	3.65E-08	1.87E-06	3.93E-07	3
GO:0031639	plasminogen activation	4.14E-08	1.87E-06	3.93E-07	3

GO:00341 14	regulation of heterotypic cell-cell adhesion	4.14E -08	1.87E-06	3.93E-07	3

Supplementary Figures

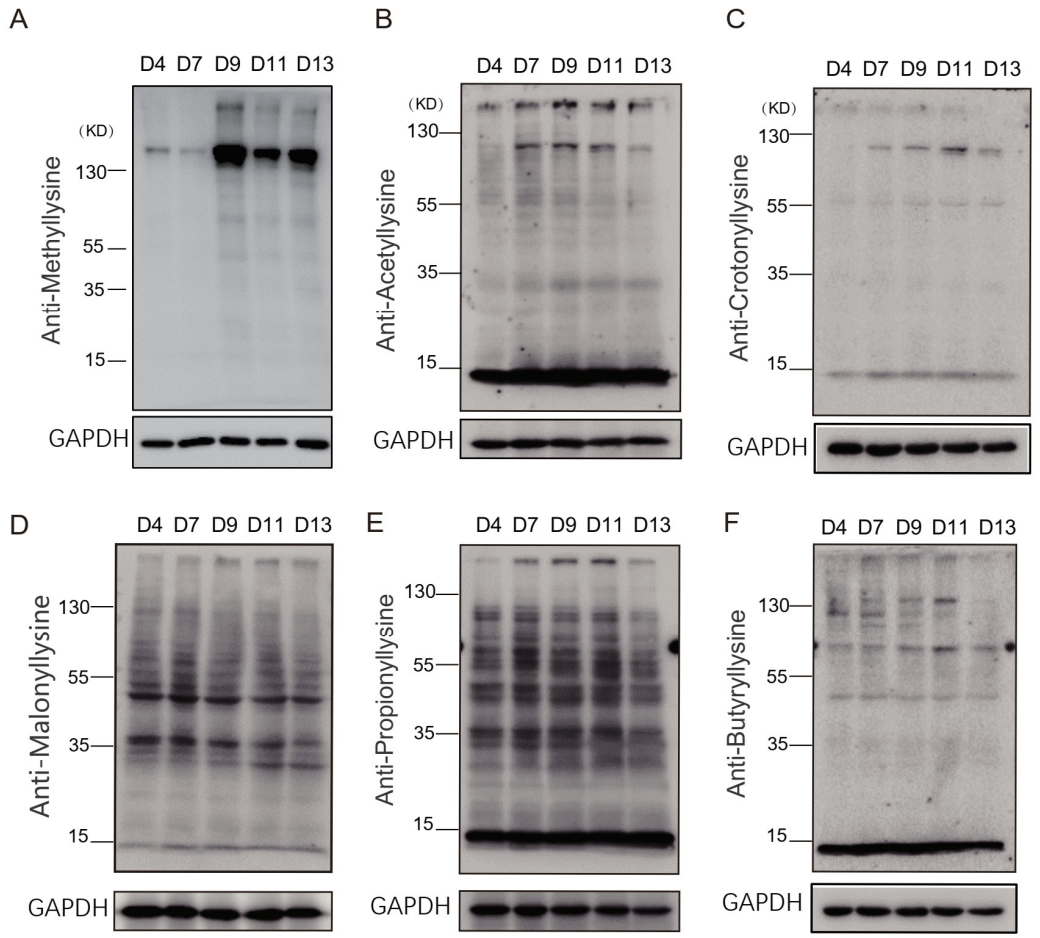

Supplementary Figure S1. Protein post-translational modifications during CD34+ cells erythroid differentiation. (A-E) CD34+ cells were collected at each developmental stage of human erythroid differentiation for cell lysis, and posttranslational modifications were detected, including methylation (A), acetylation (B), crotonylation (C), malonylation (D), propionylation (E) and butyrylation (F). GAPDH was used as a loading control.

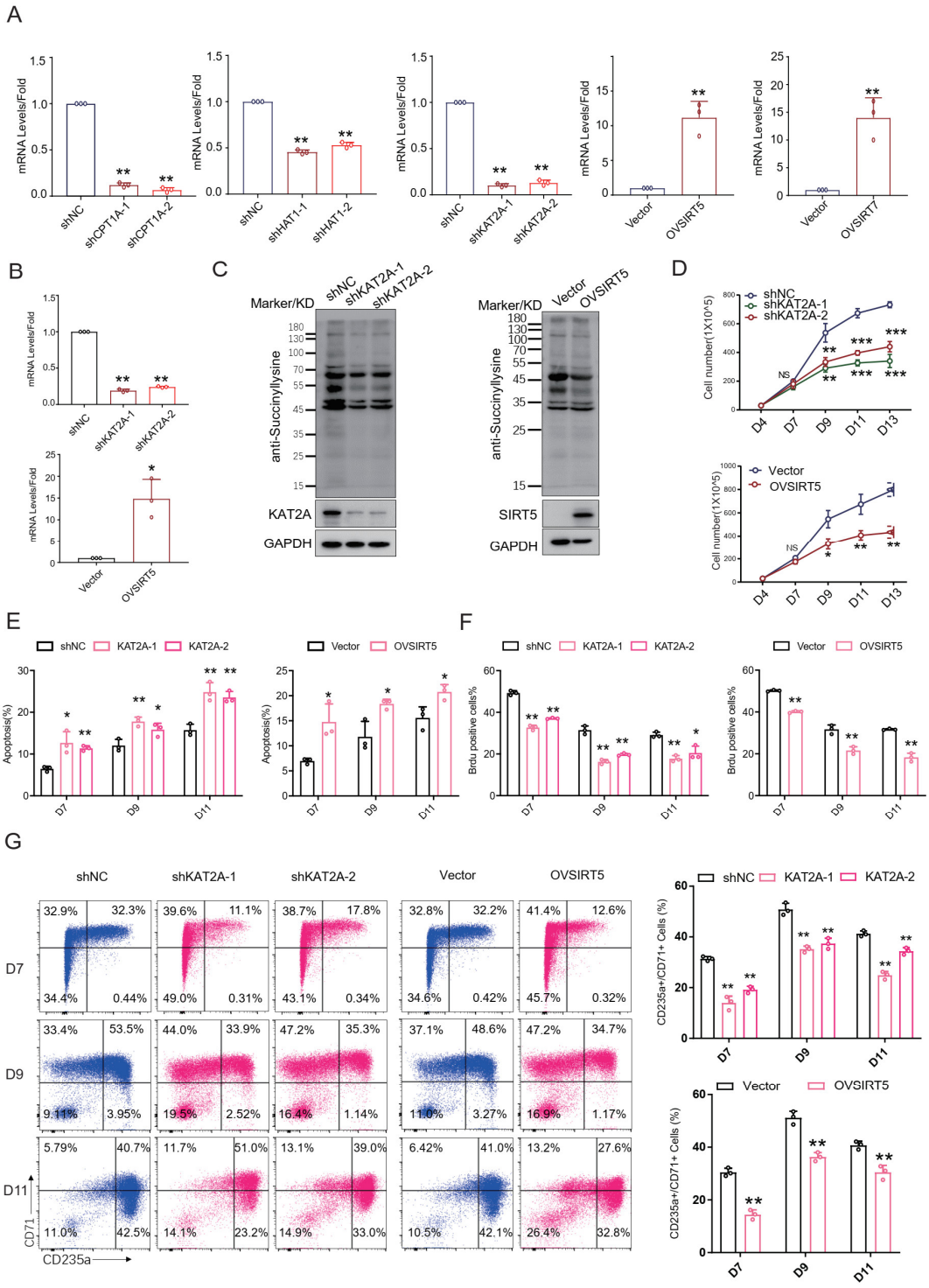
A
mRNA Levels/Fold
shNC
shCPT1A-1
shCPT1A-2
shHAT1-1
shHAT1-2
shKAT2A-1
shKAT2A-2
Vector
OVSIRT5
OVSIRT7
B
C
Marker/KD
anti-Succinyllysine
KAT2A
SIRT5
GAPDH
D
Cell number(1X10^5)
D4
D7
D9
D11
D13
NS
E
F
shNC
KAT2A-1
KAT2A-2
Apoptosis(%)
Brdu positive cells%
G
D7
D9
D11
CD71
CD235a
CD235a+/CD71+ Cells (%)
H
HAT1
CPT1A
HBA
HBB
HBG

Supplementary Figure S2. Effects of global lysine succinylation on erythroid differentiation in human CD34$^+$ cells. (A) The qRT-PCR results showing the mRNA expression levels of succinyltransferases and desuccinylases in HUDEP2 cells. (B) The qRT-PCR results showing KAT2A and SIRT5 mRNA expression levels in cultured primary erythroid cells at day 7. (C) Western blotting analysis of global lysine succinylation levels in CD34$^+$ cells infected with KAT2A knockdown and SIRT5 overexpression. (D) Cell growth curves determined by manual cell counting. (E) Cell apoptosis proportions assessed via annexin V/PI staining during erythroid differentiation. (F) Results of cell-cycle distribution obtained through BrdU assay during erythroid differentiation. (G) Flow cytometry analysis of KAT2A knockdown or SIRT5 overexpression during human erythroid differentiation at different stages in human CD34$^+$ cells. (H) Differentiation of HUDEP2 cells after infection with KAT2A or, HAT1 or CPT1A shRNA lentivirus or SIRT5 or SIRT7 overexpression virus. Western blotting images displaying KAT2A, HAT1, CPT1A, SIRT5, and SIRT7 expression in HUDEP2 cells infected with relative lentivirus, along with hemoglobin expression.

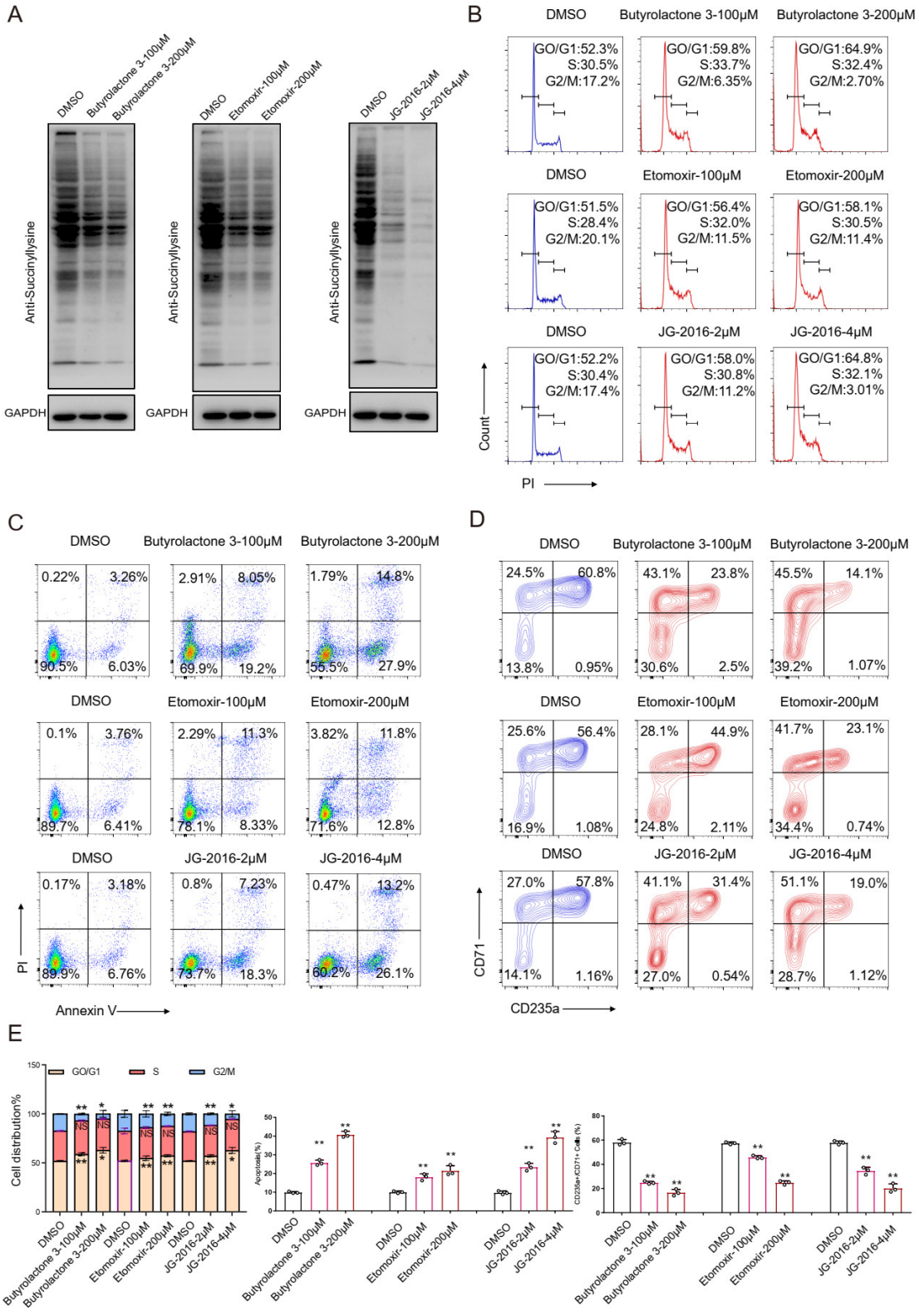

Supplementary Figure S3. Effects of global lysine succinylation on erythroid differentiation following treatment with succinyltransferase inhibitors in human CD34+ cells. (A) Western blot analysis of global lysine succinylation levels in CD34+ cells treated with

succinyltransferase inhibitors - Butyrolactone 3 (a specific small-molecule inhibitor of KAT2A), Etomoxir (an irreversible inhibitor of CPT1A), and JG-2016 (a potent inhibitor of HAT1). (B) Cell-cycle distribution during erythroid differentiation assessed through PI assay. (C) Proportions of apoptotic cells evaluated via annexin V/PI staining during erythroid differentiation. (D) Flow cytometry analysis of erythroid differentiation at various stages in human CD34+ cells treated with succinyltransferase inhibitors. (E) Cell-cycle distribution during erythroid differentiation in CD34+ cells (left), proportions of apoptotic cells during erythroid differentiation in CD34+ cells (middle), and proportions of GPA- and CD71-positive cells during erythroid differentiation in CD34+ cells (right). Statistical analysis was performed on three independent experiments, with bar plots representing the mean ± SD of triplicate samples. Significance levels are indicated as *P < 0.05, **P < 0.01, versus control, based on Student's t-test.

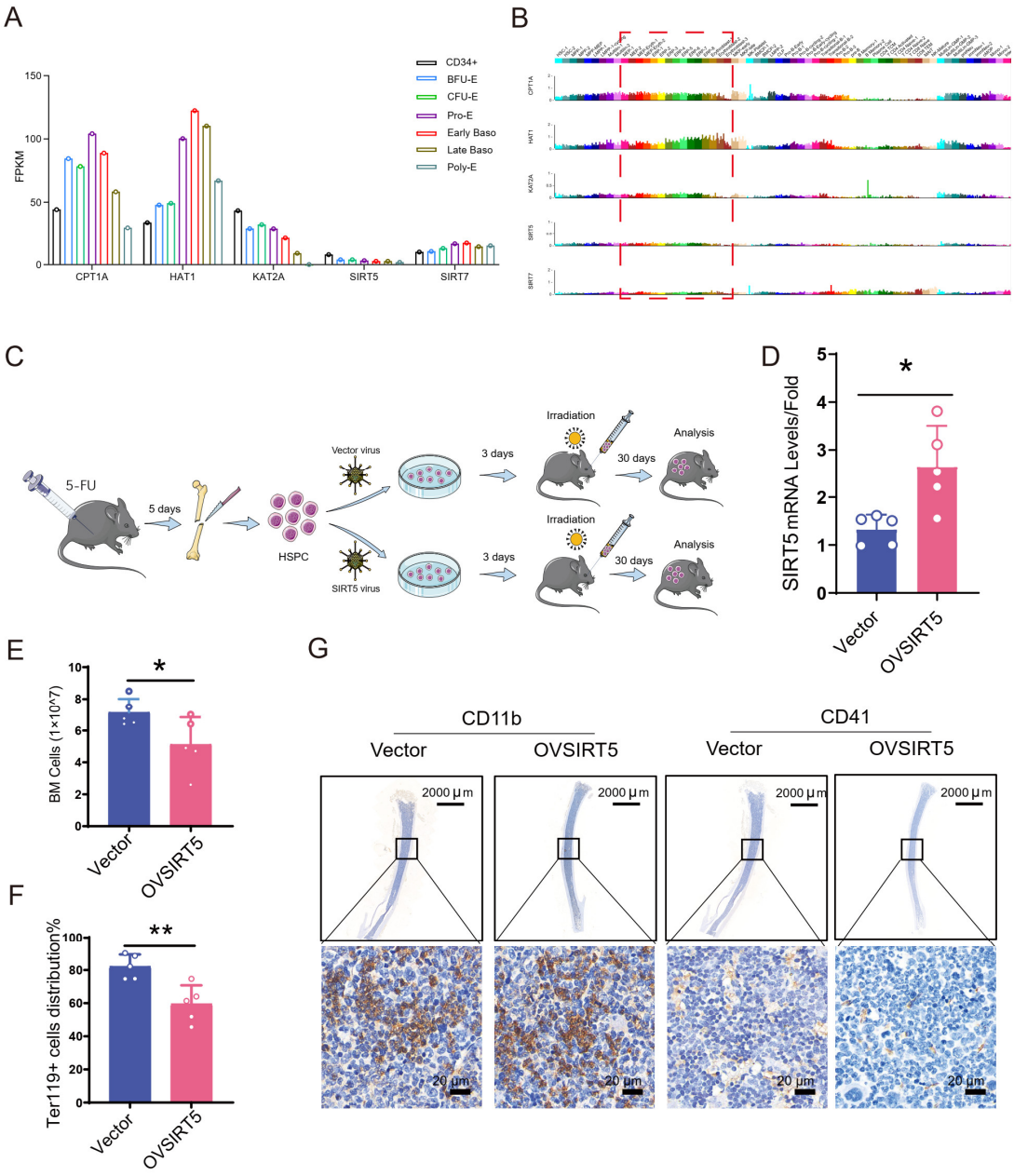

Supplementary Figure S4. Overexpression of SIRT5 impairs erythroid differentiation in vivo. (A) Expression levels of the succinylation-related enzymes during erythroid differentiation in bulk RNAseq. (B) Expression levels of the succinylation-related enzymes in the bone marrow (BM), with the red dotted box highlighting the erythroid lineages. (C) Experimental procedure for mouse bone marrow transplantation. (D) Relative mRNA levels of SIRT5 in BM cells from control and OV-SIRT5 mice, presented as the mean ± SEM (n = 5). β-actin serves as the endogenous control. (E) Upper panel: Bone marrow cell counts of control and OV-SIRT5 mice. Bottom panel: $Ter119^{+}$ cells distribution analysis based on flow cytometry results. (F) The representative vertical sections of mouse BM showing expression of

CD11b and CD41 by immunostaining.

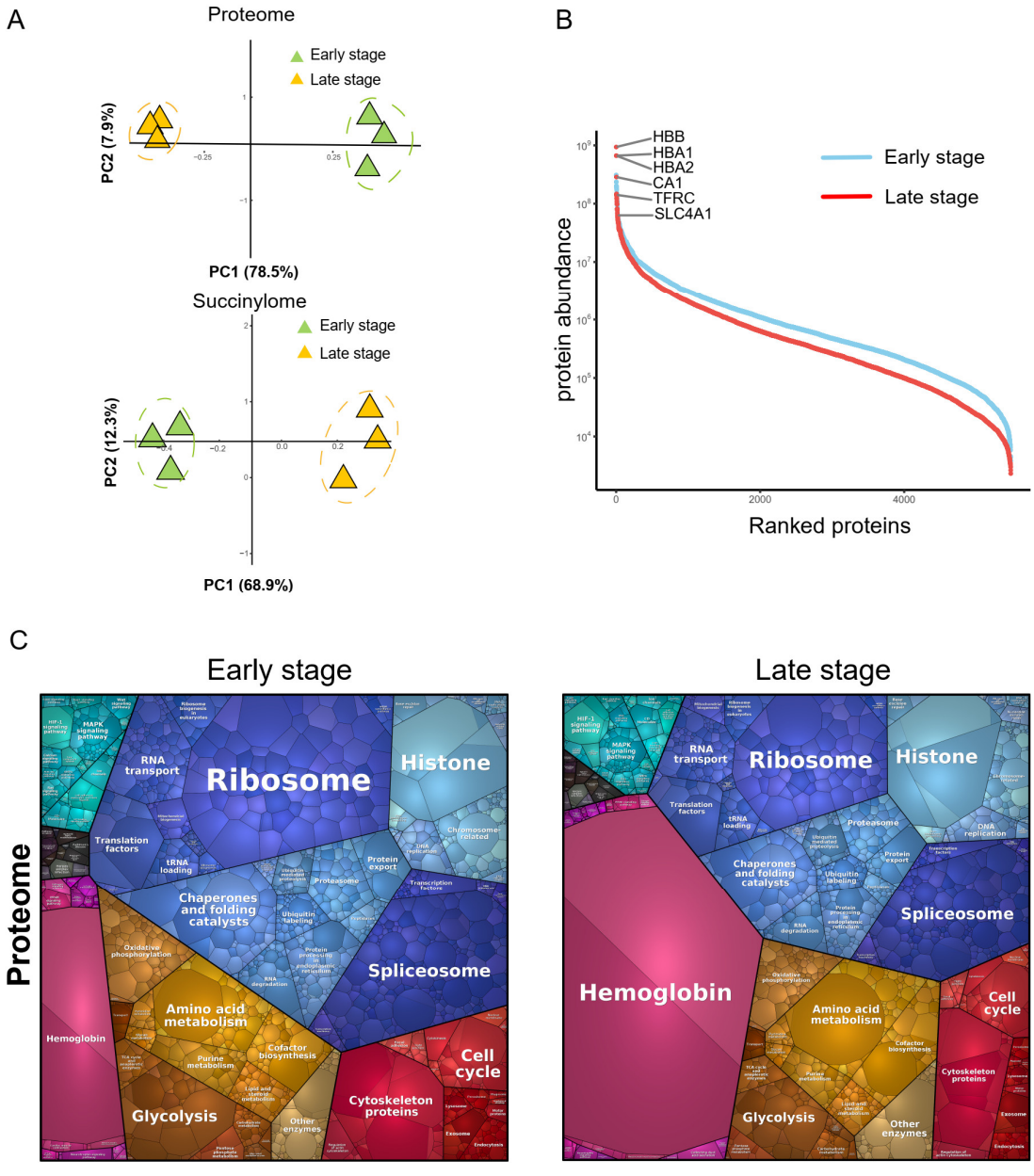

Supplementary Figure S5. Characterization of proteome and motif analysis for succinylated lysine residues. (A) Principal component analysis of all identified proteins in the proteome (upper) and succinylome (lower). (B) Distribution of proteome intensities at different erythroid differentiation stages. (C) Proteomaps demonstrate significant differences in hemoglobin levels during erythroid differentiation in proteomes.

A

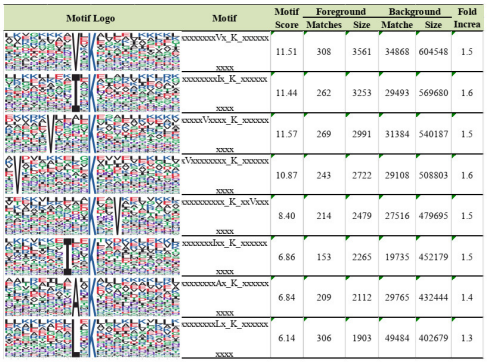

Motif Logo	Motif	Motif Score	Foreground Matches	Foreground Size	Background Matche	Background Size	Fold Increa
	xxxxxxxVx_K_xxxxxx xxxx	11.51	308	3561	34868	604548	1.5
	xxxxxxxIx_K_xxxxxx xxxx	11.44	262	3253	29493	569680	1.6
	xxxxxVxxxx_K_xxxxxx xxxx	11.57	269	2991	31384	540187	1.5
	xVxxxxxxxx_K_xxxxxx xxxx	10.87	243	2722	29108	508803	1.6
	xxxxxxxxx_K_xxVxxx xxxx	8.40	214	2479	27516	479695	1.5
	xxxxxxIxx_K_xxxxxx xxxx	6.86	153	2265	19735	452179	1.5
	xxxxxxxAx_K_xxxxxx xxxx	6.84	209	2112	29765	432444	1.4
	xxxxxxxLx_K_xxxxxx xxxx	6.14	306	1903	49484	402679	1.3

B

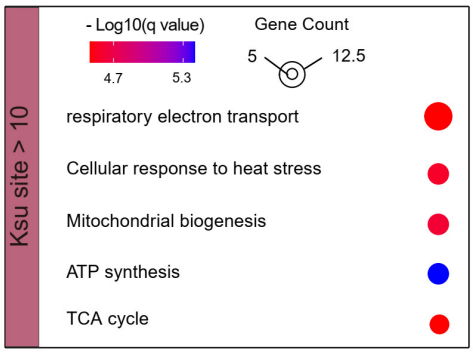

C

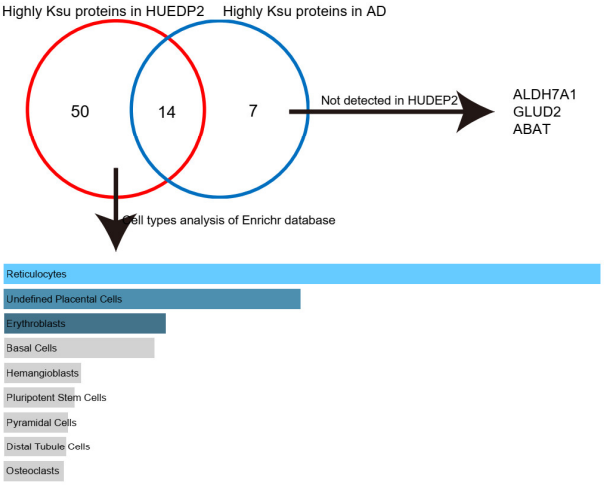

F

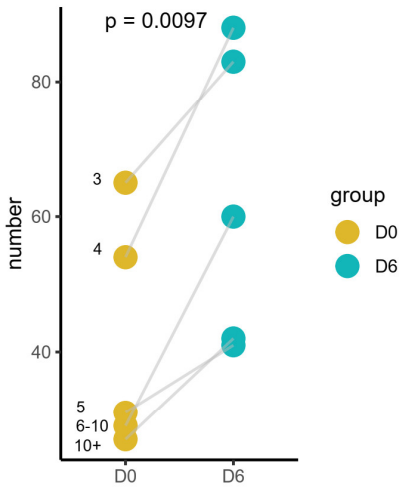

D

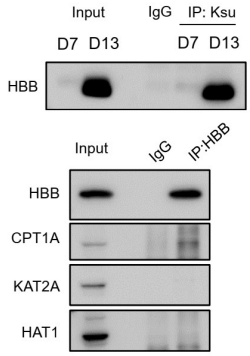

G

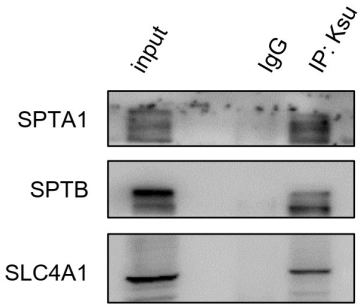

E

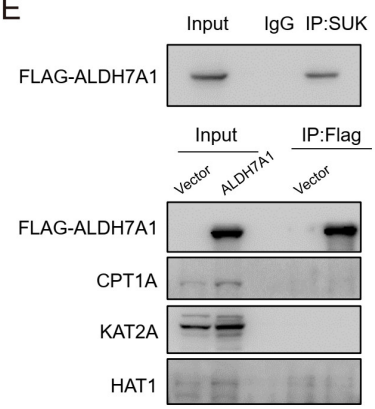

H

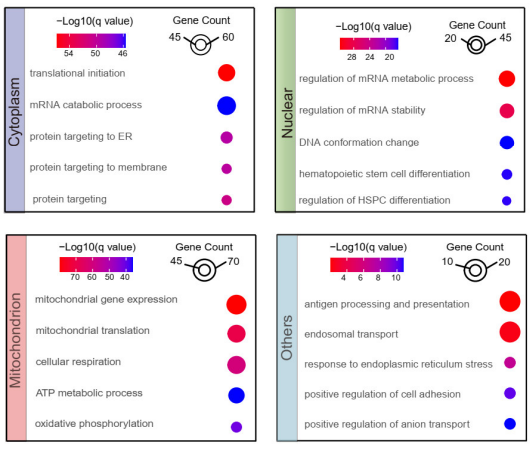

Supplementary Figure S6. Characterization of succinylome. (A) Identification of eight conserved amino acid residue frequencies around succinylated lysine residues using Motif-X during erythroid differentiation. (B) Gene Ontology Biological Process (GO-BP) enrichment analysis of proteins with >10 succinylated sites, showing significantly enriched functions. (C) The Venn plot showing the differences of succinylated proteins with >10 succinylated sites between our data with AD patients. (D) Detection of the succinylation levels of HBB and the interaction between HBB and three succinyltransferases. (E) Detection of the succinylation levels of flag-ALDH7A1 and the interaction between ALDH7A1 and three succinyltransferases. (F) Changes in the number of succinylated lysine residues from early to late-stages of erythroid differentiation. (G) Detection of the succinylation levels of SPTA1, SPTB, and SLC4A1. (H) GO analysis of succinylated proteins localized in the nucleus, cytoplasm, mitochondrion, and others showing significantly overrepresented functions.

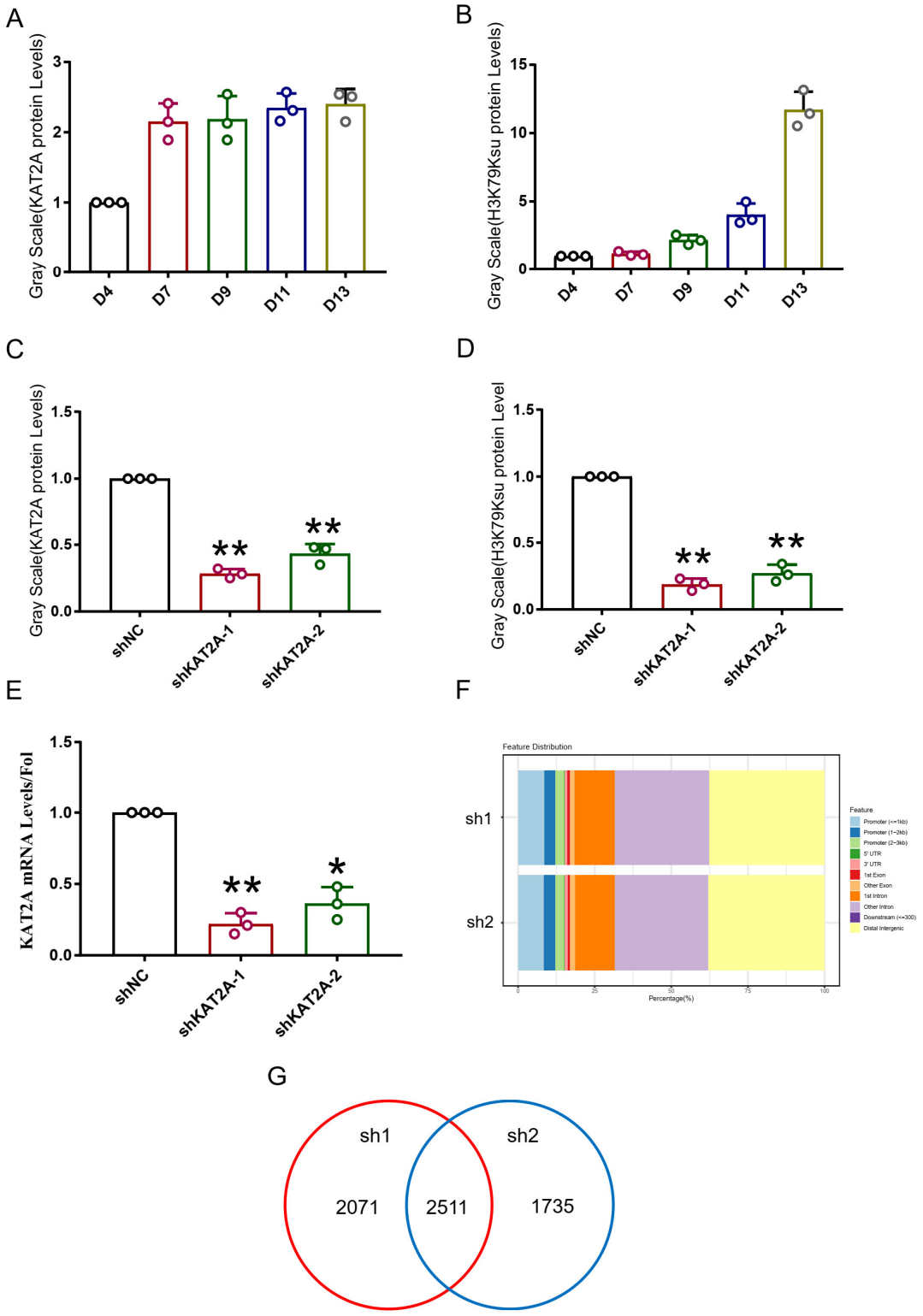

Supplementary Figure S7. The CUT&Tag analysis of H3K79Ksu in CD34⁺ cells. (A) Grayscale statistics of KAT2A expression level in erythroid differentiation. (B) Grayscale statistics of H3K79Ksu expression level in erythroid differentiation. (C) Grayscale statistics of KAT2A protein expression level. (D) Grayscale statistics of H3K79Ksu expression level. (E)

Detection of KAT2A mRNA level after knocking down KAT2A. (F) Genomic distribution of affected peaks. (G) The Venn plot showing the overlap of peak located in the promoter. Statistical analysis was performed on three independent experiments, with bar plots representing the mean ± SD of triplicate samples. Significance levels are indicated as *P < 0.05, **P < 0.01, versus control, based on Student's t-test.

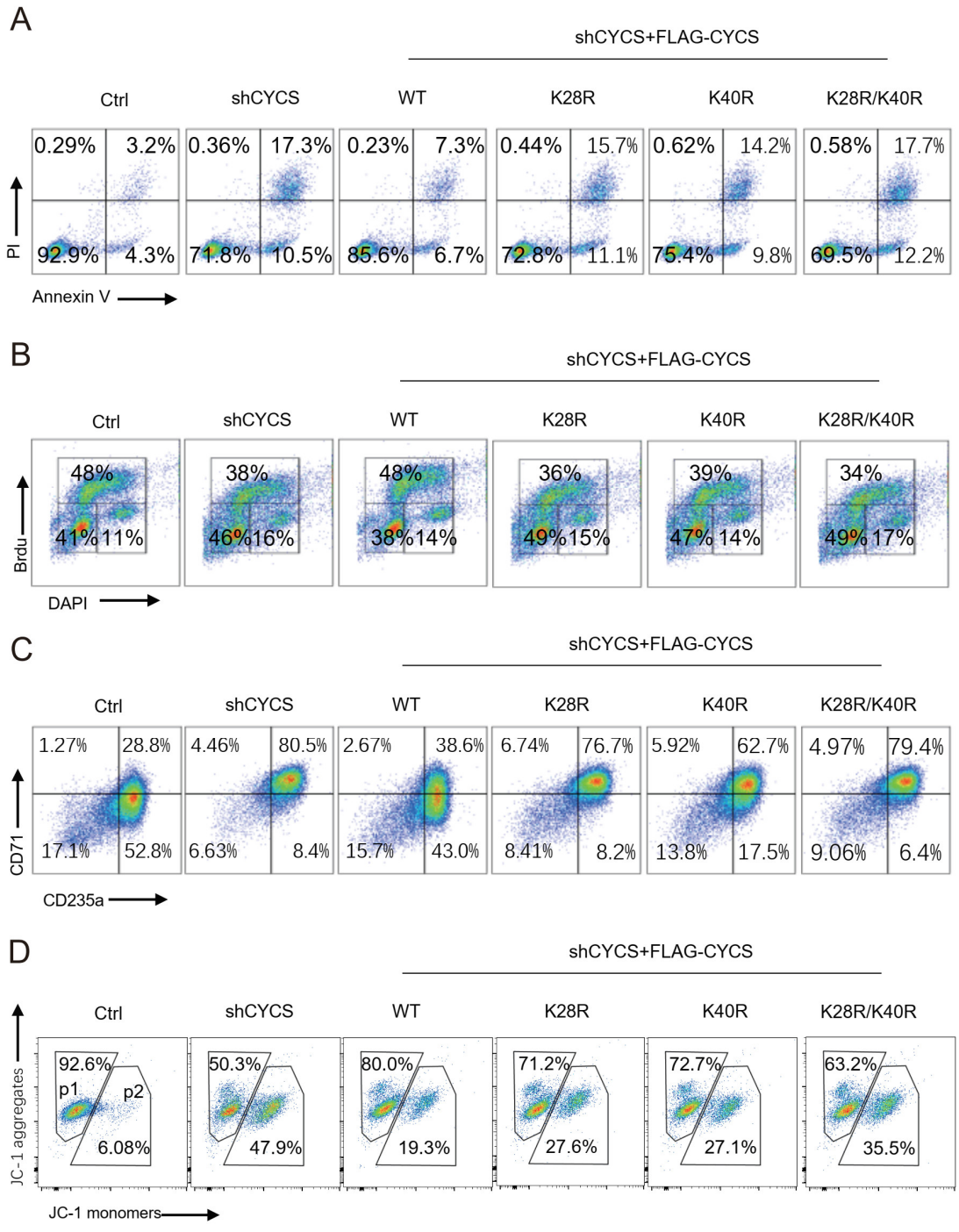

Supplementary Figure S8. The succinylation of CYCS affects erythroid differentiation. (A) Representative images of flow cytometry analysis of apoptosis by annexin V/PI staining in HUDEP2 cells. (B) Representative images of flow cytometry analysis of cell cycle by BrdU assay. (C) Representative images of flow cytometry analysis of GPA and CD71 expression. (D) Representative flow cytometry analysis of mitochondrial membrane potential using JC-1 staining.